AD-A129 682 WHITE-LIGHT OPTICAL INFORMATION PROCESSING AND HOLOGRAPHY(U) PENNSYLVANIA STATE UNIV UNIVERSITY PARK DEPT OF ELECTRICAL ENGINEERING F T YU 03 MAY 83 1/1

UNCLASSIFIED AFOSR-TR-83-0502 AFOSR-81-0148 F/G 20/6 NL

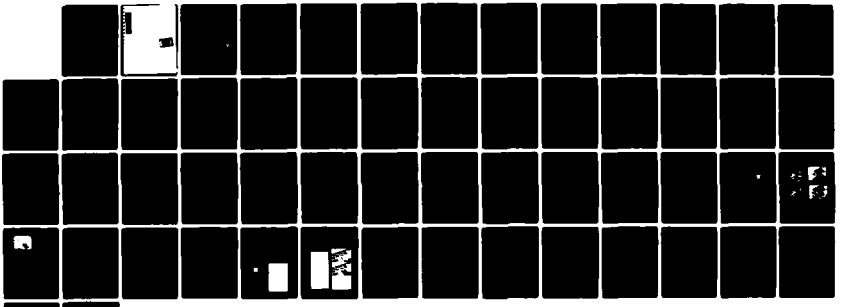

END
DATE FILMED
7 83
DTIC

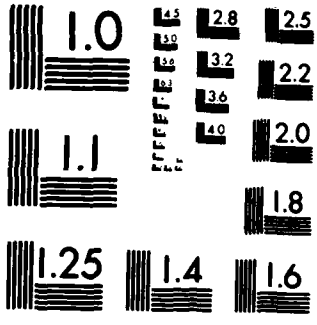

UNCLASSIFIED

SECURITY CLASSIFICATION OF THIS PAGE (When Data Entered)

REPORT DOCUMENTATION PAGE	READ INSTRUCTIONS BEFORE COMPLETING FORM
1. REPORT NUMBER: AFOSR-TR- 83-0502	2. GOVT ACCESSION NO.: AD-A129682
3. RECIPIENT'S CATALOG NUMBER	
4. TITLE (and Subtitle): White-Light Optical Information Processing and Holography	5. TYPE OF REPORT & PERIOD COVERED: Annual Report, Feb. 15, 1982-Feb. 14, 1983
	6. PERFORMING ORG. REPORT NUMBER
7. AUTHOR(s): Francis T. S. Yu	8. CONTRACT OR GRANT NUMBER(s): AFOSR - 81 - 0148
9. PERFORMING ORGANIZATION NAME AND ADDRESS: Electrical Engineering Department, The Pennsylvania State University, University Park, PA 16802	10. PROGRAM ELEMENT, PROJECT, TASK AREA & WORK UNIT NUMBERS: 6110 2F, 2305/B1
11. CONTROLLING OFFICE NAME AND ADDRESS: AFOSR/NE, Building 410, Bolling Air Force Base, Washington, D.C. 20332	12. REPORT DATE: May 3, 1983
	13. NUMBER OF PAGES: 50
14. MONITORING AGENCY NAME & ADDRESS (if different from Controlling Office)	15. SECURITY CLASS. (of this report): UNCLASSIFIED
	15a. DECLASSIFICATION DOWNGRADING SCHEDULE

16. DISTRIBUTION STATEMENT (of this Report)

Approved for public release; distribution unlimited.

17. DISTRIBUTION STATEMENT (of the abstract entered in Block 20, if different from Report)

Unlimited

18. SUPPLEMENTARY NOTES

None

19. KEY WORDS (Continue on reverse side if necessary and identify by block number)

White-Light Optical Processing, White-Light Holography, Image Subtraction, Image Deblurring, Coherence Requirement, Apparent Transfer Function, Source Encoding, Signal Sampling.

20. ABSTRACT (Continue on reverse side if necessary and identify by block number)

During the second year (FY'82) a great deal of process has been made on the white-light optical information processing and holography research program. In this period, we have evaluated the coherence requirement, source encoding, and signal sampling concept for the proposed white-light optical signal processor. We have shown that the spatial coherence requirement is governed by source distribution, while the temporal coherence requirement is controlled by spatial frequency bandwidth of the

DD FORM 1 JAN 73 1473 EDITION OF 1 NOV 65 IS OBSOLETE

UNCLASSIFIED

SECURITY CLASSIFICATION OF THIS PAGE (When Data Entered)

20. ABSTRACT (Continued)

cont

input signal and the grating sampling frequency. In order to alleviate the basic constraints of a white-light source, we have developed a source encoding and signal sampling concept, so that the information can be processed in complex amplitude for the entire spectral band of the white-light source. We have also evaluated an apparent transfer function for the proposed white-light signal processor. We have shown that the MTF is dependent upon the degree of spatial and temporal coherence. The derived apparent transfer function is very general, which can be applied to any partially coherent optical processor. Since the proposed white-light signal processor is very suitable for color image processing, we have, in this period, also demonstrated several color image processing capabilities. Among those are broadband color image deblurring and color image subtraction. From those results, we have seen high quality deblurred color images and subtracted color images can be performed by the proposed white-light optical processor. We have also in this period evaluated the primary aberrations and the bandwidth requirements for rainbow holographic processes. The conditions for the removal of the five primary aberrations are also determined.

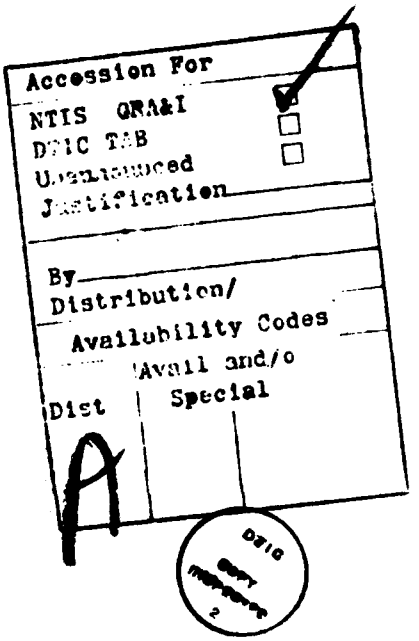

Table of Contents

I. Introduction

We have in the past year investigated several research projects on "White-Light Optical Information Processing and Holography." Our research works have been quite consistent with our AFOSR sponsored research grant reporting in various journals and conference publications. Sample copies of these papers are included in this annual report in the subsequent sections, for which to provide a concise documentation of our work. In the following sections, we will provide a general overview of our research progress made in the past twelve months and we will detail some of those research progresses. A list of publications resulting from AFOSR's support is included at the end of this report.

II. Summary and Overview

Since the invention of laser (i.e., a strong coherent source) laser has become a fashionable tool for many scientific applications particularly as applied to coherent optical signal processing. However coherent optical signal processing systems are plagued with coherent noises, which frequently limit their processing capability. As noted by the late Gabor, the Nobel prize winner in physics in 1970 for his invention of holography, the coherent noise is the number one enemy of the Modern Optical Signal Processing [1]. Aside the coherent noise, the coherent sources are usually expensive, and the coherent processing environments are very stringent. For example, heavy optical benches and dust free environments are generally required.

Recently, we have looked at the optical processing from a different standpoint. A question arises, is it necessarily true that all optical signal processing required a coherent source? The answer to this question is that there are many optical signal processings that can be carried out

by a white-light source [2]. The advantages of the proposed white-light signal processing technique are: 1. It is capable of suppressing the coherent noise; 2. White-light sources are usually inexpensive; 3. The processing environments are not critical; 4. The white-light system is relatively easy and economical to maintain; and 5. The white-light processor is particularly suitable for color image processing.

There is however a basic different approach toward a coherent and a white-light processor. In coherent processing, virtually no one seems to care about the coherence requirements, since the laser provides a strong coherent source. However, in white-light processing, the knowledge of the coherence requirement is usually needed.

In white-light processing we would approach the problem backward. First, we should know what is the processing operation we wish to perform: Is it a 1-D or 2-D processing? Is the signal filtering a point or point-pair concept? What is the spatial bandwidth of the signal? etc. Then with these knowledge, we would be able to evaluate the coherence requirements at the Fourier and at the input planes. From the evaluated results, we would be able to design a signal sampling function and a source encoding function to obtain these requirements. The objective of using a signal sampling function is to achieve a high degree of temporal coherence in Fourier plane so that the signal can be processing in complex amplitude, for the entire spectral band of a white-light source. And for the source encoding is to alleviate the constraints of an extended white-light source.

In the following sections, we shall highlight some of the research done during the past year effort on the white-light signal processing.

2.1 Coherence Requirement (See Section III)

Our research in the past year period has included the evaluation of the coherent requirement for white-light signal processing [3]. The mutual intensity function for a partially coherent light is used to develop an expression for the output intensity distribution for a broad-band optical information processor. The coherence requirement for smeared image deblurring and image subtraction is then determined using the intensity distribution.

We have shown that the temporal and spatial coherence requirements for some partially coherent optical processing operations, namely, image deblurring and image subtraction, can be determined in terms of the output intensity distribution. For image deblurring the temporal coherence requirement depends on the ratio of the deblurring width to the smeared length of the blurred image. To obtain a higher degree of deblurring a narrower spectral width of the light source is required. For example, if the deblurring ratio $\Delta w/w$ is 0.1, the spectral width, $\Delta\lambda$, should be < 640 Å.

For the spatial coherence requirement the image deblurring depends on both the deblurring ratio $\Delta w/w$ and the smeared length w. If the deblurring ratio $\Delta w/w = 1/10$ and $w = 1$ mm, a slit source < 0.26 mm should be used. For a smeared image deblurring operation the constraints of the temporal and spatial coherence requirements are not critical, which can be achieved in practice.

For image subtraction, the temporal coherence requirement is determined by the highest spatial frequency and the separation of the input object transparencies. If the separation and spatial frequency of the input transparencies are high, a narrower spatial bandwidth of the light source is required.

For spatial coherence requirement, the modulation transfer function, which determines the contrast of the subtracted image, depends on the ratio of the slit width to the spatial period of the encoding mask, ie., d/D. If the ratio d/D is low, a higher contrast subtracted image can be obtained. For example, with d/D = 0.05, a relatively higher MTF = 0.85 can be obtained. Compared with the image deblurring operations, the coherence requirements are more stringent for the subtraction process.

Finally, we have concluded that, the solution to the coherence requirement for partially coherent processing is not restricted to the application of the deblurring and subtraction operation, but may also be applied to any other optical processing operation.

2.2 Apparent Transfer Function (See Section IV).

We have in the past year period evaluated an apparent transfer function for our white-light optical signal processing system [4].

The nonlinear behavior of the partially coherent optical processor, when considering either intensity or amplitude distribution input signals, necessitates the use of the apparent transfer function to accurately predict the system response. We have derived the general formulas for MTF in terms of the theory of partially coherent light. These derivations indicate the dependence of MTF upon the degree of spatial coherence (i.e., the source size) as well as the degree of temporal coherence (i.e., the source spectral bandwidth). MTF has been shown to be less dependent upon the spatial coherence requirement as compared to its relationship with the temporal coherence requirement.

It has been oted that the spatial bandwidth of our optical processor is primarily dependent upon the size of the filter Δx, where the filter is placed in the Fourier plane. The transfer systems bandwidth may be

increased by using a larger spatial filter Δx. However, the size of the filter is selected such that $\Delta x = p_o f \Delta\lambda$, which is linearly related to the spatial frequency of grating, the focal length of the transform lens and the spectral width of the light source. A narrow spectral band $\Delta\lambda$ is necessary for most partially coherent optical information processing operations. In order to achieve the required $\Delta\lambda$ for a wide strip of spatial filter Δx in the spatial frequency plane, a diffraction grating of sufficiently high frequency p_o at the input plane is needed. For example, for partially coherent processing with a white light source, a set of narrow spectral band filters, each with a spectral bandwidth $\Delta\lambda$, can be used in the spatial frequency plane.

Finally, we conclude that the apparent transfer function which we have obtained is rather general and may be applied to any partially coherent optical processing system.

2.3 Source Encoding and Signal Sampling (See Section V).

We have in the past year developed a concept of source encoding and signal sampling for our white-light signal processor [5]. We have shown that the advantage of source encoding is to provide an appropriate spatial coherence function at the input plane so that the signal processing can be carried out by an extended incoherent source. The effect of the signal sampling is to achieve the temporal coherence requirement at the Fourier plane so that the signal can be processed in complex amplitude. If the filtering operation is two-dimensional, a multi-spectral-band 2-D filters should be utilized. If the filtering operation is one-dimensional, a fan-shape filter can be used.

In short, one should carry out the processing requirements backward for a white-light processing. With these processing requirements (e.g.,

operation, temporal and spatial coherence requirements), multi-spectral-band or broad-band filter, signal sampling function, and source encoding mask can be synthesized. Thus the signal processing can be carried out in complex amplitude over the whole-spectral band of the white-light source.

2.4 Broadband Image Deblurring (See Reference 6)

In this period of research, we have shown a broadband color image deblurring technique utilizing a white-light source [6]. This broad spatial band deblurring technique utilized a grating base method to obtain a dispersed smeared image spectra in the Fourier plane so that the deblurring operation can be taken placed in complex amplitude for the entire visible wavelengths. To perform this complex amplitude deblurring for the entire spectral band of the light source, we have shown that a fan-type deblurring filter to compensate the scale variation of the smeared signal spectra due to wavelength dispersion can be utilized. To alleviate the low transmission efficiency of the deblurring filter, we synthesized the deblurring filter with the combination of a broadband phase filter and a fan-shaped amplitude filter. The broad spectral band phase filter is synthesized by optical coating techniques, while the fan-shaped amplitude filter is obtained by a 1-D coherent processing technique.

By comparison of the results obtained by the broadband image deblurring with the narrow spectral band and coherent techniques, we have seen that the results obtained by the broadband deblurring offer a higher image quality. We have also shown that the broadband deblurring technique is very suitable for color image deblurring. We have provided several color image deblurring results obtained by the broadband deblurring technique. From these color deblurred images we have seen that the

fidelity of the color reproduction is very high and the quality of deblurred image is rather good. Although there is some degree of color blur due to chromatic aberration of the transform lenses, it can be eliminated by utilizing higher-quality achromatic transform lenses.

Further improvements of the deblurring can also be obtained by utilizing a blazed grating to achieve a higher smeared spectral diffraction efficiency so that a wider spatial band deblurring filter can be used to achieve a higher degree of deblurring.

2.5 Color Image Subtraction (See Section VI)

We have also in this period accomplished a research project on color image subtraction with extended incoherent sources [7]. We have introduced a source encoding technique to obtain a point-pair spatial coherence function for the subtraction operation. The basic advantage of source encoding is to increase the available light power for the image subtraction operation, so that the inherent difficulty of obtaining incoherent point sources can be alleviated. Since the technique uses incoherent sources, the annoying coherent artifact noise can be suppressed. We would see that the concept of color image subtraction may also be extended to the use of white-light source, for which a program is currently under investigation. In experimental demonstrations, we have shown that color subtracted images can be easily obtained by this incoherent subtraction technique. Since virtually all images of natural objects are color, the technique may offer a wide range of practical applications.

2.6 Rainbow Holographic Aberrations (See Section VII)

In this period, we have also theoretically evaluated the primary aberrations and the bandwidth requirements for rainbow holographic

processes [8]. The results obtained for the rainbow holographic process are rather general, for which the conventional holographic image resolution, aberrations, and bandwidth requirements, can be derived. The conditions for the elimination of the five primary rainbow holographic aberrations are also given. These conditions may be useful for the application of obtaining a high-quality rainbow hologram image. In terms of bandwidth requirements, we have shown that the bandwidth requirement for a rainbow holographic construction is usually several orders lower than that of a conventional holographic process. Therefore, a lower-resolution recording medium can generally be used for most of the rainbow holographic constructions.

2.7 Remarks

We have demonstrated in the past twelve months that the proposed white-light optical signal processor is very suitable for color image processings, which is one step closer to the reality of the practical optical image processing. As compared with the conventional coherent optical signal processor and the electronic digital counterparts, the white-light signal processor offers the advantage of

1. Cost effective in operation,
2. Simplicity of system maintenance,

and 3. Suitability for color signal processing.

However, there is a basic different approach toward a coherent and a white-light processor. In white-light processing, the knowledge of the coherence requirement is usually needed. With the knowledge of the temporal coherence requirement in the Fourier plane and the spatial coherence requirement at the input plane, a signal sampling function and a source encoding function can be utilized to achieve these requirements such that the signal processing can be carried out by an extended white-

light source. In other words, one should carry out the processing requirements backward for a white-light processing, so that the signal can be processing in complex amplitude rather than in intensity.

In short, we have shown that the white-light processor on one hand can process the signal in complex amplitude like a coherent processor, on the other hand it suppresses the coherent noise like an incoherent processor.

2.8 Future Research

Our future research is expected to follow the general direction addressed in the proposal. Attention will be given in the following:

1. To develop a real-time processing capability for the proposed white-light processing technique.
2. To carry out various experimental demonstrations for the real-time processing mode.
3. To develop a real-time color image processing technique.
4. To carry out the real-time color image processing capabilities as applied to color image transformation, restoration, detection, encoding, etc.
5. To develop a technique of synthesizing a multi-wavelength complex spatial filter that is suitable for white-light signal detection system.
6. To carry out a computer generated spatial filter program for the broadband optical detection and recognition problem.
7. Provides experimental demonstrations of the principles and processing operation that we propose.
8. Extension of the source encoding technique for image subtraction utilizing a broadband white-light source.

9. The implementation of natural sun light for the proposed processing system.

In summary, our goal is to develop a full research program on the white-light signal processing technique which has the capability of carrying out all the major processing operations that a coherent optical processor can offer. This white-light optical processing system is vitally essential in many areas of monochrome and color signal processings. We are confident that this white-light processing technique will provide a step toward the research and development of white-light and sunlight optical computers.

2.9 References

1. D. Gabor, IBM, J. Res. Develop, 14, 509 (1970).
2. F. T. S. Yu, Optical Information Processing, Wiley-Interscience, NY, 1983.
3. S. L. Zhuang and F. T. S. Yu, Appl. Opt., 21, 2587 (1982).
4. S. L. Zhuang and F. T. S. Yu, Appl. Phy., B28, 359 (1982).
5. F. T. S. Yu, S. L. Zhuang and S. T. Wu, Appl. Phy., B27, 99 (1982).
6. S. L. Zhuang, T. H. Chao, and F. T. S. Yu, J. Opt. Soc. Am., 72, 1721 (1982).
7. F. T. S. Yu and S. T. Wu, J. Opt., 13, 183 (1982).
8. Y. W. Zhang, W. G. Zhu and F. T. S. Yu, Appl. Opt., 22, 164 (1983).

SECTION III

Coherence Requirement

Reprinted from Applied Optics, Vol. 21, page 2587, July 15, 1982

Coherence requirements for partially coherent optical processing

S. L. Zhuang and F. T. S. Yu

The mutual intensity function for a partially coherent light is used to develop an expression for the output intensity distribution for a broadband optical information processor. The coherence requirement for smeared image deblurring and image subtraction is then determined using the intensity distribution. We also quantitatively show the dependence of coherence criteria on the spectral bandwidth, the source size, deblurring width, spatial frequency, and the separation of input object transparencies.

I. Introduction

Optical systems perform myriad sophisticated information processing operations using coherent light.[1-3] However, coherent systems are susceptible to coherent artifact noise, which frequently limits their processing capability. The use of incoherent light alleviates the noise problem,[4-7] usually at the cost of a lowered signal-to-noise ratio due to dc bias. Various workers have studied optical systems which employ (a) a totally incoherent source[8,9] or (b) a broadband source with reduced coherence.[10] The question to be addressed in the paper is, to what degree can we relax the coherence requirement without sacrificing the overall results of the processing system? We use Wolf's[11] theory of partially coherent light to develop the necessary coherence criteria for an optical processor. The results are used to discuss the temporal and spatial coherence requirements for the specific problems of image deblurring and image subtraction.

The nature of optical processing operations governs the spatial and temporal coherence requirements necessary to obtain satisfactory results. As system configuration varies from one application to the other it is desirable to develop a generalized function for the system output intensity expressed as a function of the spectral and spatial bandwidths.

Consider the partially coherent optical processing system[12-14] in Fig. 1. Let the source plane P_0 be that of an incoherent spatially extended light source (i.e., white-light source) with an intensity distribution $\gamma(x_0,y_0)$. The input plane P_1 contains the signal transparency and also a coding mask (e.g., a sinusoidal grating) if needed.[12-14] Let the complex amplitude transmittance at this plane be $t(u,v)$. Its spectrum may then be processed in complex amplitude by placing a complex spatial filter $f(x,y)$ in the Fourier plane. The theory of partially coherent light can be used now to write the output intensity distribution,[11,16]

$$I(u',v') = \int_{\lambda_0-\Delta\lambda/2}^{\lambda_0+\Delta\lambda/2} \iint_{-\infty}^{\infty} \gamma(x_0,y_0)S(\lambda)C(\lambda) \times \left| \iint_{-\infty}^{\infty} T(x+x_0, y+y_0;\lambda)f(x,y) \times \exp\left[-j\frac{2\pi}{\lambda f}(xu'+yv')\right]dxdy\right|^2 dx_0dy_0d\lambda, \quad (1)$$

where $S(\lambda)$ and $C(\lambda)$ are defined to be the relative spectral intensity of the light source and the relative spectral response sensitivity of the detector, respectively. $T(x,y;\lambda)$ is the Fourier spectrum of the input transparency for wavelength λ of the light source. The integration is performed over the spectral bandwidth $\Delta\lambda$ of the light source, λ_0 being its center wavelength.

In the following sections we shall use the output intensity distribution given by Eq. (1) to evaluate the coherence requirement for image deblurring and image subtraction of a partially coherent optical information processor.

II. Coherence Requirement for Image Deblurring

A photographic image deblurring technique employing a white-light source has been described in previous papers.[13,15] We had briefly stated that the coherence requirements depend on the smeared length of the object and the size and spectral bandwidth of the light source.[17] We shall now discuss the temporal and spatial coherence requirements for image deblurring separately.

The authors are with Pennsylvania State University, Electrical Engineering Department, University Park, Pennsylvania 16802.
Received 8 March 1982.
0003-6935/82/142587-09$01.00/0.

A. Temporal Coherence Requirement

We consider a spectrally broadband point source for which the intensity distribution can be expressed by a Dirac δ function, i.e., $\gamma(x_0,y_0) = \delta(x_0,y_0)$. The spectral distribution is uniform over the bandwidth [$s(\lambda) = k$, a constant]. If the smeared length W is known *a priori*, the output deblurred image irradiance can be derived from Eq. (1) as

$$I(u',v') = \int_{\lambda_l}^{\lambda_h} |A(u',v';\lambda)|^2 d\lambda, \tag{2}$$

where λ_l and λ_h are the extreme lower and upper wavelengths of the light source;

$$A(u',v';\lambda) = \int_{-\infty}^{\infty} T(x,y;\lambda) f(x,y) \exp\left[-j\frac{2\pi}{\lambda f}(xu' + yv')\right] dxdy \tag{3}$$

is the output complex light distribution of the deblurred image due to wavelength λ; $T(x,y;\lambda)$ is the Fourier spectrum of the input blurred transparency $t(u,v)$ due to λ; and $f(x,y)$ is the deblurring filter.

We note that, if the input blurred image is superimposed with a sinusoidal phase grating, the blurred image spectrum will disperse into rainbow colors in the Fourier plane thus allowing a stripwise design of deblurring filter for each narrow spatial band in the Fourier plane. It is evident that the temporal coherence requirement is limited by the narrow spectral band (i.e., narrow strip) of the deblurring filter. If the input object is a linear smeared image, a fan-shaped deblurring filter can be used to compensate the wavelength variation.[13,15] Since each of the narrow strip deblurring filters is spatial frequency-limited over a narrow spectral band, the coherence requirement for each narrow strip filter can be equivalently analyzed as the case without the input phase grating (i.e., the coding mask).

Since the image deblurring takes place at every image point the linear blurred image transparency may be represented as

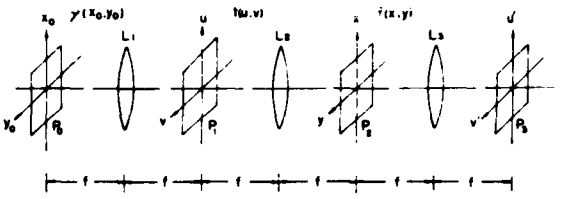

Fig. 1. Partially coherent optical processing system: P_0, source plane; P_1, input plane; P_2, Fourier plane; P_3, output plane; L, achromatic lenses.

$$t(u,v) = \text{rect}(u/W), \tag{4}$$

$$T(x,y;\lambda) = \mathcal{F}[t(u,v)] = \text{sinc}\left(\frac{W}{\lambda f}x\right), \tag{5}$$

where f is the focal length of the achromatic transform lenses, and

$$\text{rect}(u/W) = \begin{cases} 1 & |u| \le W/2, \\ 0 & \text{otherwise.} \end{cases} \tag{6}$$

The deblurring filter is thus

$$f(x;\lambda_0) = \frac{1}{T(x;\lambda_0)} = \frac{1}{\text{sinc}\left(\frac{W}{\lambda_0 f}x\right)}, \tag{7}$$

where λ_0 is the center wavelength of the light source, and for simplicity we have adopted a 1-D notation. The corresponding deblurred image is given by

$$\begin{aligned} A(u';\lambda) &= \int_{-\infty}^{\infty} T(x;\lambda) f(x;\lambda_0) \exp\left(-j\frac{2\pi}{\lambda f}xu'\right) dx \\ &= \text{rect}(u'/W) * \int_{-\infty}^{\infty} \frac{1}{\text{sinc}\left(\frac{W}{\lambda_0 f}x\right)} \exp\left(-j\frac{2\pi}{\lambda f}xu'\right) dx, \end{aligned} \tag{8}$$

where $*$ denotes the convolution operation. By a straightforward but tedious calculation, illustrated in the Appendix, the deblurred image of Eq. (8) can be shown to be

$$A(u';\lambda) = \begin{cases} \dfrac{4\lambda_0 f}{\pi} \displaystyle\sum_{n=1}^{2m} (-1)^n \sin\frac{\pi n\lambda_0}{\lambda} \sin\frac{2\pi n\lambda_0}{\lambda W} u' \cdot \text{sgn}(u'), & \text{for } |u'| > W/2, \\ -\dfrac{4\lambda_0 f}{\pi} \displaystyle\sum_{n=1}^{2m} (-1)^n \cos\frac{\pi n\lambda_0}{\lambda} \cos\frac{2\pi n\lambda_0}{\lambda W} u', & \text{for } |u'| \le W/2. \end{cases} \tag{9}$$

where the series converges for $2m \gg 1$. In the final result it can be shown that the output image irradiance is given by

$$\begin{aligned} I^{(1)}(u',\Delta\lambda) = \frac{2\lambda_0^2 f^2}{\pi^2} \sum_n \sum_{n'} \sum_{l=1}^{8} (-1)^{n+n'+l} \{ &3|\lambda_a^{-3} \cos[a^l_{nn'}(u')\lambda_a]| \\ &- \lambda_b^{-3} \cos[a^l_{nn'}(u')\lambda_b]| - 6\,|a^l_{nn'}(u')|\,|\lambda_a^{-2} \sin[a^l_{nn'}(u')\lambda_a]| \\ &- \lambda_b^{-2} \sin[a^l_{nn'}(u')\lambda_b]| - 6\,|a^l_{nn'}(u')|^2\,|\lambda_a^{-1} \cos[a^l_{nn'}(u')\lambda_a]| \\ &- \lambda_b^{-1} \cos[a^l_{nn'}(u')\lambda_b]| - 6\,|a^l_{nn'}(u')|^3\,[\text{Si}(\lambda_a) - \text{Si}(\lambda_b)]\}, \quad \text{for } |u'| > W/2, \end{aligned} \tag{10}$$

$$\begin{aligned} I^{(2)}(u',\Delta\lambda) = \frac{2\lambda_0^2 f^2}{\pi^2} \sum_n \sum_{n'} \sum_{l=1}^{8} (-1)^{n+n'} \{ &6|a^l_{nn'}(u')|^3\,[\text{Si}(\lambda_a) - \text{Si}(\lambda_b)] \\ &+ 6|a^l_{nn'}(u')|^2\,|\lambda_a^{-1} \cos[a^l_{nn'}(u')\lambda_a] - \lambda_b^{-1} \cos[a^l_{nn'}(u')\lambda_b]| \\ &+ 6|a^l_{nn'}(u')|\,|\lambda_a^{-2} \sin[a^l_{nn'}(u')\lambda_a] - \lambda_b^{-1} \sin[a^l_{nn'}(u')\lambda_b]| \\ &- 3|\lambda_a^{-3} \sin[a^l_{nn'}(u')\lambda_a] - \lambda_b^{-3} \cos[a^l_{nn'}(u')\lambda_b]|\}, \quad \text{for } |u'| \le W/2. \end{aligned} \tag{11}$$

For these equations, note that

$$\lambda_a = \lambda_0/(\lambda_0 - \Delta\lambda), \tag{12}$$

$$\lambda_b = \lambda_0/(\lambda_0 + \Delta\lambda), \tag{13}$$

$$\mathrm{Si}(x) \triangleq \int_0^x \frac{\sin y}{y}\,dy, \tag{14}$$

$$a_{nn'}^{(1)}(u') = \pi(n - n')(1 - 2u'/W),$$

$$a_{nn'}^{(3)}(u') = \pi(n - n')(1 + 2u'/W),$$

$$a_{nn'}^{(5)}(u') = \pi(n + n')(1 - 2u'/W),$$

$$a_{nn'}^{(7)}(u') = \pi(n + n')(1 + 2u'/W), \tag{15}$$

and

$$a_{nn'}^{(2)}(u') = \pi[n(1 - 2u'/W) - n'(1 + 2u'/W)],$$

$$a_{nn'}^{(4)}(u') = \pi[n(1 + 2u'/W) - n'(1 - 2u'/W)],$$

$$a_{nn'}^{(6)}(u') = \pi[n(1 - 2u'/W) + n'(1 + 2u'/W)],$$

$$a_{nn'}^{(8)}(u') = \pi[n(1 + 2u'/W) + n'(1 - 2u'/W)]. \tag{16}$$

Equations (10)–(16) provide the mathematical basis for the evaluation of the temporal coherence requirement of a smeared image deblurring process. Plots of the normalized deblurred image irradiance, defined as a function of u' and the bandwidth $\Delta\lambda$, are shown in Fig. 2. $\lambda_0 = 5461$ Å was used for the calculation. It is evident that if the light source is strictly coherent (i.e., $\Delta\lambda = 0$), the deblurred point image is infinitesimal. Also note that the degree of deblurring decreases as the temporal coherence of the light source reduces. The deblurred length ΔW represents the spread of the deblurred image irradiance. It is formally defined as the separation between the 10% points of $I(u')$. The deblurred length ΔW can be shown to decrease monotonically with $\Delta\lambda$. Plots of ΔW as a function of the spectral bandwidth $\Delta\lambda$ for various values of smeared length W are shown in Fig. 3. It may be shown that the deblurred length ΔW is linearly proportional to the smear length W for a given value of $\Delta\lambda$. The greater the smear, the more difficult the deblurring process. In principle this may be corrected by decreasing the spectral bandwidth of the light source. Table I numerically summarizes the preceding analysis. The value of $\Delta\lambda$ can be regarded as the temporal coherence requirement for the deblurring process.

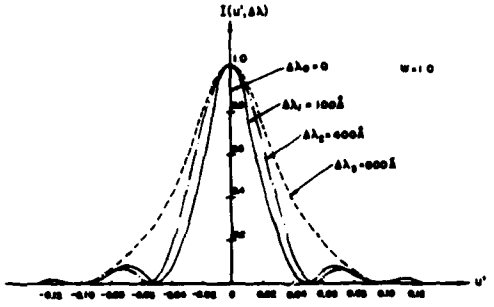

Fig. 2. Output intensity distribution of the deblurred image. $\Delta\lambda$, spectral bandwidth of the light source; W, smeared length.

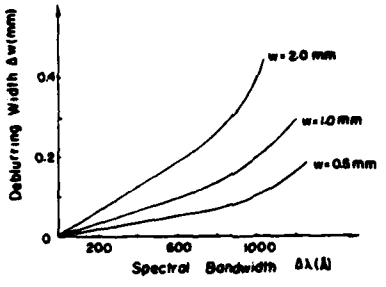

Fig. 3. Plots of the deblurring width ΔW as a function of the spectral bandwidth of the light source $\Delta\lambda$ for various values of smeared light W.

Table I. Effect of Temporal Coherence Requirement

$\Delta W/W$	1/20	1/15	1/10	1/8	1/5
$\Delta\lambda$(Å)	270	400	640	750	990

B. Spatial Coherence Requirement

The relationship between the source size and the image intensity distribution is the key factor in the calculation of the degree of spatial coherence requirement for a particular image deblurring system. The following analysis assumes a 1-D processor for simplicity.

Assume the intensity distribution of the light source is given by

$$\gamma(x_0) = \mathrm{rect}(x_0/\Delta s). \tag{17}$$

If an extended monochromatic light source is used, the output intensity distribution of Eq. (1) becomes

$$I(u') = \int_{-\infty}^{\infty} \mathrm{rect}(x_0/\Delta s)\,|A(u', x_0; \lambda)|^2 dx_0, \tag{18}$$

where

$$A(u', x_0; \lambda) = \int_{-\infty}^{\infty} \mathrm{sinc}\left[\frac{W}{\lambda f}(x + x_0)\right] \exp\left(-j\frac{2\pi}{\lambda f}xu'\right) dx \cdot \int_{-\infty}^{\infty} \frac{1}{\mathrm{sinc}\left(\frac{W}{\lambda f}x\right)} \exp\left(-j\frac{2\pi}{\lambda f}xu'\right) dx, \tag{19}$$

and $*$ denotes the convolution operation.

Equation (19) can be reduced to the form of

$$A(u',x_0;\lambda)=\begin{cases}2f\lambda_0 j\sum_{n=1}^{\infty}(-1)^n n\exp(j2\pi\alpha u'/W)\left[\exp\left(j\frac{2\pi n}{W}u'\right)\operatorname{sinc}(\alpha+n)-\exp\left(-j\frac{2\pi n}{W}u'\right)\operatorname{sinc}(\alpha-n)\right], & \text{for } |u'|>W/2,\\ \frac{2f\lambda_0}{\pi}\sum_{n=1}^{\infty}(-1)^n n\exp(j2\pi\alpha u'/W)\left(\frac{1}{\alpha-n}|1-\exp[j2\pi(\alpha-n)u'/W]\cos\pi(\alpha-n)|\right) & \\ +\frac{1}{\alpha+n}|1-\exp[j2\pi(\alpha+n)u'/W]\cos\pi(\alpha+n)|, & \text{for } |u'|\le W/2,\end{cases}\tag{20}$$

where $\alpha = x_0W/(\lambda f)$.

By substituting Eq. (20) into Eq. (2) and performing the required mathematical evaluation, the deblurred image irradiance is found to be (a) for $|u'| > W/2$:

$$I^{(1)}(u',\Delta s)=\frac{16f^3\lambda_0^3}{W\pi^2}\sum_n\sum_{n'}|\Phi^{(1)}_{nn'}(\Delta s)\cos[2\pi(n-n')u'/W]+\Phi^{(2)}_{nn'}(\Delta s)\cos[2\pi(n+n')u'/W]|.\tag{21}$$

Note that, in this equation, the following parameters may be defined:

$$S_j(m,\Delta s)=S_i\,|2\pi[\bar\alpha(\Delta s)-m)]|-S_i|2\pi[-\bar\alpha(\Delta s)-m]|.\tag{22}$$

In addition define

$$C_j(m,\Delta s)=C_i[2\pi|\bar\alpha(\Delta s)+m|]-C_i[2\pi|\bar\alpha(\Delta s)-m|],\tag{23}$$

where

$$\operatorname{Si}(x)=\int_0^x\frac{\sin\beta}{\beta}d\beta,\qquad C_i(x)=\int_x^\infty\frac{\cos\beta}{\beta}d\beta,\qquad \bar\alpha(\Delta s)=\Delta SW/(2\lambda f),\tag{24}$$

and

$$\Phi^{(1)}_{nn'}(\Delta s)=\frac{nn'}{n'-n}\left\{|n\left[\frac{n+\bar\alpha(\Delta s)}{n-\bar\alpha(\Delta s)}\right]-[(-1)^nC_j(n,\Delta s)-(-1)^{n'}C_j(n',\Delta s)]\right\},\tag{25}$$

$$\Phi^{(2)}_{nn'}(\Delta s)=\frac{nn'}{n'+n}\left\{|n\left[\frac{n+\bar\alpha(\Delta s)}{n-\bar\alpha(\Delta s)}\right]-[(-1)^nC_j(n,\Delta s)-(-1)^{n'}C_j(n',\Delta s)]\right\}.$$

(b) for $|u'| \le W/2$ we may similarly show

$$I^{(2)}(u',\Delta s)=\frac{16\lambda_0^3f^3}{W\pi^2}\sum_n\sum_{n'}|\Phi^{(3)}_{nn'}(\Delta s)+\Phi^{(4)}_{nn'}(\Delta s)\sin[2\pi(n'-n)u'/W]+\Phi^{(5)}_{nn'}(\Delta s)\cos[2\pi(n'-n)u'/W]+\Phi^{(6)}_{nn'}(\Delta s)\cos[2\pi(n+n')u'/W]|,\tag{26}$$

where

$$\begin{aligned}\Phi^{(3)}_{nn'}(\Delta s)&=(-1)^n\frac{2n}{n^2-n'^2}|n\left[\frac{n-\bar\alpha(\Delta s)}{n+\bar\alpha(\Delta s)}\right]\\&\quad+(-1)^n\frac{n}{n^2-n'^2}[C^+_k(n',\Delta s)+C^-_k(n',\Delta s)],\\ \Phi^{(4)}_{nn'}(\Delta s)&=\frac{n'}{n^2-n'^2}[S^+_k(n,\Delta s)+S^-_k(n,\Delta s)],\\ \Phi^{(5)}_{nn'}(\Delta s)&=(-1)^{n+1}\frac{n'}{n^2-n'^2}[C^+_k(n,\Delta s)+C^-_k(n,\Delta s)]\\&\quad+\frac{2}{n'-n}\left\{|n\left[\frac{n+\bar\alpha(\Delta s)}{n-\bar\alpha(\Delta s)}\right]+[C_j(n,\Delta s)-C_j(n',\Delta s)]\right\},\\ \Phi^{(6)}_{nn'}(\Delta s)&=\frac{1}{n+n'}\left\{|n\left[\frac{n-\bar\alpha(\Delta s)}{n+\bar\alpha(\Delta s)}\right]-[C_j(n,\Delta s)+C_j(n',\Delta s)]\right\}.\end{aligned}\tag{27}$$

and

$$\begin{aligned}S^\pm_k(m,\Delta s)&=S_i|\pi(2u'/W\pm1)[\bar\alpha(\Delta s)+m]|-S_i|\pi(2u'/W\pm1)[-\bar\alpha(\Delta s)+m]|,\\ C^\pm_k(m,\Delta s)&=C_i[\pi|2u'/W\pm1||\bar\alpha(\Delta s)+m|]-C_i[\pi|2u'/W\pm1||-\bar\alpha(\Delta s)+m|].\end{aligned}\tag{28}$$

Thus the spatial coherence requirement of an image deblurring process may be evaluated by using Eqs. (21) and (26). The output intensity distribution of this process is plotted in Fig. 4.

Recall the definition of the deblurred length ΔW stated to be the separation between the 10% points of the image irradiance $I(u')$. Figure 5 shows the plots of ΔW as a function of the source size Δs and the smear length W. From this figure it can be seen that when the spatial width of the light source increases beyond a critical size Δs_c, the deblurred length becomes inde-

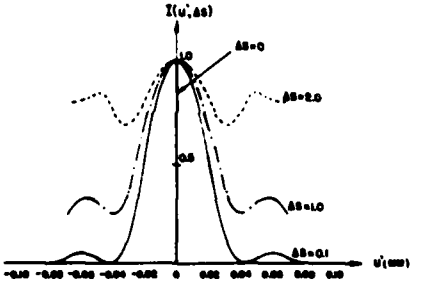

Fig. 4. Output intensity distribution of the deblurred image for various values of the source size Δs.

pendent of Δs and equal to W. Table II provides a brief numerical summary of the key parameters for the determination of the spatial coherence in image deblurring. From this table it is evident that the spatial coherence requirement is inversely proportional to the smear length W. That is, the longer the smearing length, the smaller the source size is required.

III. Coherence Requirement for Image Subtraction

Wu and Yu[18] have reported an image subtraction procedure employing an extended incoherent source and a source encoded mask. Here, we shall discuss the temporal and spatial coherence requirements of the image subtraction process and show that they depend on the size and spectral bandwidth of the light source.

The output intensity distribution can be derived by calculating the propagation of the mutual coherence function through an optical system that utilizes an encoded extended source. With reference to Fig. 6 the encoded source intensity distribution may be described by

$$\gamma(x_0,y_0) = \mathrm{rect}(x_0/d) * \sum_{n=-N}^{N} \delta(x_0 - nD), \tag{29}$$

where * denotes the convolution operation, D is the spacing of the $2N + 1$ encoding slits, and d is the width of each slit. Image subtraction is essentially a 1-D processing operation and will be analyzed as such.

The encoded mutual coherence function at the input plane P_1 can be written

$$J(u_1 - u_2;\lambda) = \int_{-\infty}^{\infty} \gamma(x_0,y_0) \exp\left[-j \frac{2\pi}{\lambda f}(u_1 - u_2)x_0\right] dx_0, \tag{30}$$

or, in regard to Eq. (29),

$$J(u_1 - u_2;\lambda) = \sum_{n=-N}^{N} \mathrm{sinc}\frac{d(u_1 - u_2)}{\lambda f} \exp\left[-j \frac{2\pi}{\lambda f}(u_1 - u_2)nD\right]. \tag{31}$$

As shown in Fig. 6 two object transparencies, $A(u)$ and $B(u)$, are placed at the input plane P_1. These can be represented by

$$t(u) = A(u - H) + B(u + H), \tag{32}$$

where the separation between transparencies is $2H$. The mutual coherence function in the P_2 plane is simply the Fourier transform of $J_0(u_1 - u_2;\lambda)$ convolved with the spectrum of the amplitude transmittance function $t(u)$. The image subtraction process requires that a sinusoidal grating of spatial frequency ω_0 be placed in the Fourier plane. Thus the mutual coherence function behind this grating is given by

$$J(x_1,x_2;\lambda) = \mathcal{F}\{J(u_1 - u_2;\lambda)t(u_1)t^*(u_2)\}(1 + C\sin 2\pi\omega_0 x_1) \times (1 + C\sin 2\pi\omega_0 x_2). \tag{33}$$

A final Fourier transform operation due to wavelength λ will give the intensity distribution at the output plane P_3:

$$I(u';\lambda) = \iint_{-\infty}^{\infty} J(x_1,x_2;\lambda) \exp\left[-j \frac{2\pi}{\lambda f}(x_1 - x_2)u'\right] dx_1 dx_2, \tag{34}$$

or

Table II. Effect of Spatial Coherence Requirement

Δs mm \ $\frac{\Delta W}{W}$	1/20	1/15	1/10	1/5
0.5 mm	0.2	0.38	0.6	0.92
1 mm	0.1	0.18	0.26	0.40
2 mm	0.05	0.08	0.12	0.18

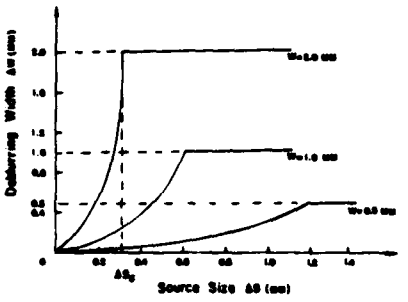

Fig. 5. Plots of the deblurring width as a function of the source size for various values of the smear length W.

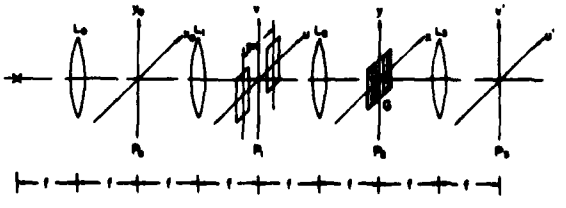

Fig. 6. Partially coherent optical processing system for image subtraction: S_1, light source; P_0, encoded extended source plane; P_1, input plane; P_2, Fourier plane; P_3, output plane; L, achromatic lenses.

$$I(u';\lambda) = N[|A(u'-H)|^2 + |B(u'+H)|^2] + \frac{NC^2}{4}|2\sin(2d\omega_0)$$
$$\times \mathrm{Re}[A(u'-H+\lambda f\omega_0)B(u'+H-\lambda f\omega_0)] - |A(u'-H+\lambda f\omega_0)|^2$$
$$- |B(u'+H-\lambda f\omega_0)|^2 - |A(u'-H-\lambda f\omega_0)|^2 - |B(u'+H+\lambda f\omega_0)|^2\}, \quad (35)$$

where Re denotes the real part of $\{\ \}$. From the above equation we see that there are six diffracted image terms at the output plane. If we only consider the diffracted images around the optical axis of the output plane, from Eq. (35) we have

$$I^{(0)}(u';\lambda) = |A(u'-H+\lambda f\omega_0)|^2 - 2\,\mathrm{sinc}(2d\omega_0)$$
$$\times \mathrm{Re}[A(u'-H+\lambda f\omega_0)B(u'+H-\lambda f\omega_0)]$$
$$+ |B(u'+H-\lambda f\omega_0)|^2. \quad (36)$$

where $\omega_0 = H/\lambda f$.

If the slit size d equals zero, the analysis reduces to the case of strictly spatial coherence with the intensity distribution given by

$$I^{(0)}(u';\lambda)|_{d=0} = [A(u') - B(u')]^2. \quad (37)$$

Equations (36) and (37) show that a high-contrast subtracted image requires a strictly spatial coherent system, and that the image quality will decrease as the slit width d increases.

To analyze the case of partial coherence assume the light source has a uniform spectral bandwidth and that the spectral response of the detector is also uniform [i.e., $s(\lambda) = k$; $C(\lambda) = k$]. Then the image intensity distribution at the output plane may be given by

$$I^{(0)}(u') = \int_{-\Delta\lambda/2}^{\Delta\lambda/2} |A(u'+\lambda' f\omega_0)|^2 - 2\,\mathrm{sinc}(2d\omega_0)$$
$$\times \mathrm{Re}[A(u'+\lambda' f\omega_0)$$
$$\times B(u'-\lambda' f\omega_0)] + |B(u'-\lambda' f\omega_0)|^2 d\lambda', \quad (38)$$

where $\lambda' = \lambda - \lambda_0$, λ_0 is the center frequency, and $\Delta\lambda$ is the spectral bandwidth of the source; ω_0 is the spatial frequency of the grating. Equation (38) may be simplified by using a Taylor series expansion for the input object functions. Thus for

$$A(u'+\lambda' f w_0) \approx A(u') + \sum_{m=1}^{\infty} \frac{1}{m!} A^{(m)}(u')(\lambda' f w_0)^m,$$
$$B(u'-\lambda' f w_0) \approx B(u') + \sum_{m=1}^{\infty} \frac{1}{m!} B^{(M)}(u')(\lambda' f w_0)^m, \quad (39)$$

where

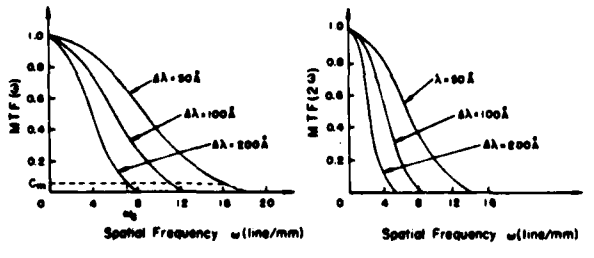

Fig. 7. Apparent modulation transfer function for a partially coherent image subtraction: (a) basic frequency; (b) second harmonic.

$$A^{(m)}(u') = d^m A(u')/du'^m,$$
$$B^{(m)}(u') = d^m B(u')/du'^m. \quad (40)$$

we find that

$$I^{(0)}(u') = [|A(u)|^2 - 2\,\mathrm{sinc}(2dw_0)A(u')B(u') + |B(u')|^2]\Delta\lambda$$
$$+ \sum_{\substack{m=\text{even} \\ m\neq 0}} \frac{1}{2^{m-1}(m+1)!}(fw_0)^m[A^{(m)}(u')$$
$$- \mathrm{sinc}(2dw_0)B^{(m)}(u')]$$
$$\times [A(u') + B(u')](\Delta\lambda)^{m+1}$$
$$+ \sum_{\substack{m \\ m\neq 0}} \sum_{\substack{m' \\ m'\neq 0 \\ m+m'=\text{even}}} \frac{1}{2^{(m+m'-1)}(m+m'+1)m!m'!}$$
$$\times (fw_0)^{m+m'}[A^{(m)}(u')A^{(m')}(u')$$
$$- (-1)^{m'}\,\mathrm{sinc}(2dw_0)A^{(m)}(u')B^{(m')}(u')$$
$$+ (-1)^{m+m'}B^{(m)}(u')B^{(m')}(u')](\Delta\lambda)^{m+m'+1}. \quad (41)$$

This equation shows that a high-contrast subtracted image can be obtained with object transparencies of moderately low spatial frequency content. In addition this equation may be used to compute the spectral requirement of the light source.

An example analysis will be presented to develop the modulation transfer function (MTF) equations. These will be used to determine the temporal and spatial coherence requirements of the image subtraction process. Assume the input object transparencies are given by

$$A(u) = 1, \qquad B(u) = \tfrac{1}{2}[1 + C_0\cos(2\pi\omega u)], \quad (42)$$

where C_0 is the contrast of the sinusoidal grating.

In the case of strictly coherence (i.e., $\Delta\lambda = d = 0$) the subtracted image produces a contrast reversed image with intensity distribution

$$I_0(u') = [A(u') - B(u')]^2, \quad (43)$$

or

$$I_0(u') = \frac{1}{4} - \frac{C_0^2}{8} - \frac{C_0}{2}\cos(2\pi\omega u') - \frac{C_0^2}{8}\cos 2\pi(2\omega)u'. \quad (44)$$

For a partially coherent case due to Eq. (38), the intensity of the subtracted image can be shown to be

$$I_0(u') = \left[\frac{5}{4} - \frac{C_0^2}{8} - \mathrm{sinc}(2d\omega_0)\right]\Delta\lambda + C_0[\tfrac{1}{2} - \mathrm{sinc}(2d\omega_0)]$$
$$\times \mathrm{sinc}(f\omega\omega_0\Delta\lambda)\Delta\lambda\cos(2\pi\omega u')$$
$$+ \frac{C_0^2}{8}\mathrm{sinc}(2f\omega\omega_0\Delta\lambda)\Delta\lambda\cos 2\pi(2\omega)u'. \quad (45)$$

Note the addition of a second harmonic term $[\cos 2\pi(2\omega)u']$ to the basic frequency. The MTF is defined as the ratio of the contrasts of the input and output sinusoidal objects. These are given by

$$\mathrm{MTF}(w) = \frac{[1 - 2\,\mathrm{sinc}(2d\omega_0)](2 - C_0^2)\,\mathrm{sinc}(f\omega\omega_0\Delta\lambda)}{10 - C_0^2 - 8\,\mathrm{sinc}(2d\omega_0)}, \quad (46)$$

$$\mathrm{MTF}(2w) = \frac{(2 - C_0^2)\,\sin(2f\omega\omega_0\Delta\lambda)}{10 - C_0^2 - 8\,\mathrm{sinc}(2d\omega_0)}. \quad (47)$$

As previously stated Eqs. (46) and (47) will allow the evaluation of the temporal and spatial coherent requirements for image subtraction.

A. Temporal Coherence Requirement

The case of strictly spatial coherence will be discussed first. This requires that the slit width d approach zero. Equations (46) and (47) will then become

$$\mathrm{MTF}(\omega) = \mathrm{sinc}(f\omega\omega_0\Delta\lambda), \quad (48)$$

$$\mathrm{MTF}(2\omega) = \mathrm{sinc}(2f\omega\omega_0\Delta\lambda). \quad (49)$$

The normalized MTF curves of the basic and harmonic frequencies are shown in Fig. 7. It is obvious that the contrast of the subtracted image decreases monotonically as a function of the object spatial frequency. However, the MTF of the subtracted image decreases as the spectral bandwidth of the light source increases. In other words the quality of the subtracted image improves as the spectral bandwidth of light source and the spatial frequency of the object decrease.

Let ω_c be the cutoff spatial frequency where the MTF decreases to a minimum value C_m as shown in Fig. 7. The value C_m depends on the maximum resolution of the output recording material. Figure 8 shows the functional relationship of the cutoff frequency ω_c and the spectral width $\Delta\lambda$ for various values of C_m. It is possible to determine the spectral bandwidth requirement $\Delta\lambda$ from this figure. The relationship between the cutoff frequency ω_c, the spectral width $\Delta\lambda$, and the separation between two input transparencies H is shown in Fig. 9. Note that the spectral bandwidth required for a given cutoff frequency decreases with increasing separation H. Table III illustrates the dependence of $\Delta\lambda$ on ω_c and H. The focal length of the Fourier transform lens selected is $f = 300$ mm for calculation. It is clear from the table that, as the spatial frequency and object separation increase, the spectral bandwidth of the light source must decrease.

B. Spatial Coherence Requirement

Consider the case of perfect temporal coherence (i.e., $\Delta\lambda = 0$) and partially spatial coherence, where Eqs. (46) and (47) are of the form

$$\mathrm{MTF}_1 = \frac{(2 - C_0^2)[1 - 2\,\mathrm{sinc}(2d\omega_0)]}{10 - C_0^2 - 8\,\mathrm{sinc}(2d\omega_0)}, \quad (50)$$

$$\mathrm{MTF}_2 = \frac{2 - C_0^2}{10 - C_0^2 - 8\,\mathrm{sinc}(2d\omega_0)}. \quad (51)$$

Note that the MTFs are independent of the object's spatial bandwidth. The above equations are, however, dependent on the slit width d. This requires that the grating be precisely designed to match the separation of the object transparencies, i.e.,

$$\omega_0 = H/(\lambda f_0). \quad (52)$$

The plots of the MTF vs the separation H for Eqs. (50)

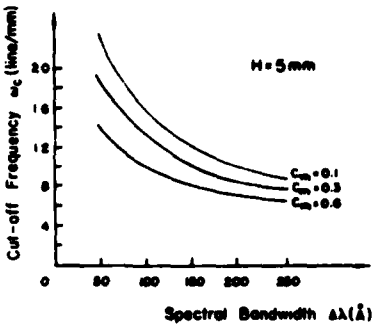

Fig. 8. Relationship between the cutoff frequency ω_0 and the spectral bandwidth of the light source $\Delta\lambda$ for different minimum desirable contrasts C_m.

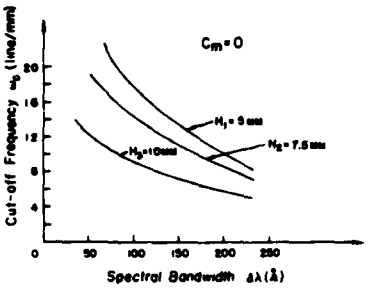

Fig. 9. Relationship between the cutoff frequency and the spectral bandwidth of the light source $\Delta\lambda$ for various values of separation H. $2H$ is the main separation between the input object transparencies.

Table III. Temporal Coherence Requirement for Different ω_c and H.

$\Delta\lambda$(Å) / ω_c(l/mm) / H(mm)	4	8	12	16	18
5.0	240	135	92	67	52
7.5	176	92	62	45	32
10.0	130	70	45	32	17

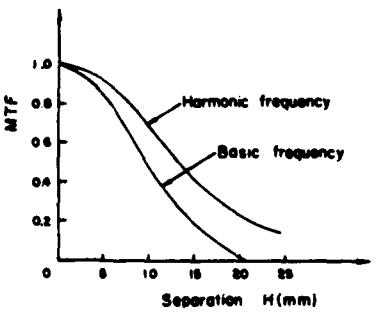

Fig. 10. Apparent modulation transfer function vs the separation H for different desirable contrasts C_m.

and (51) are shown in Fig. 10. It is obvious that to obtain a high-contrast subtraction image the separation H must be reduced. However, decreasing the separation between the object transparencies limits the size of input objects to be processed. The relationship between the MTF, the object transparency separation H, and the slit width d is numerically presented in Table IV, where the focal length of the Fourier transform lens was assumed to be 300 mm.

Note that this table indicates the necessity of a very narrow source size to achieve an adequate MTF. However, to obtain a high-intensity narrow source size is difficult to achieve in practice. The problem can be solved considerably if source encoding techniques for image subtracting are used.[17,18]

A multislit source encoding mask is used for this illustration. The spatial period of the encoding mask should be precisely equal to that of the diffraction grating G (i.e., $D = 1/\omega_0$). The spatial coherence requirement, although independent of the slit size, is governed by the ratio of the slit width to the spatial period of the encoding mask, i.e., d/D. The ratio d/D must be relatively small to achieve a high degree of spatial coherence. The dependence of the MTF on d/D is shown in Fig. 11. It is obvious that the subtraction effect ceases when the MTF approaches zero, i.e., $d/D = 0.3$. A few numerical examples are presented in Table V.

Table IV. Source Size for Image Subtraction Under Different MTF and Separation H

d(mm) \ H(mm) / MTF	5.0	7.5	10.0
0.1	0.0076	0.005	0.0038
0.3	0.0052	0.0035	0.0026
0.6	0.0031	0.0021	0.0015

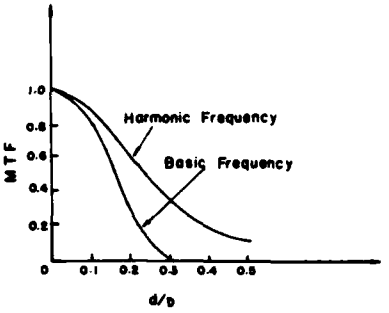

Fig. 11. Relationship between MTF (ω), MTF (2ω), and the ratio of the slit width to spatial period d/D.

Table V. Spatial Coherence Requirement for Various d/D

d/D	0.05	0.10	0.20	0.30
MTF	0.85	0.57	0.18	0.006

IV. Summary

We have shown that the temporal and spatial coherence requirements for some partially coherent optical processing operations, namely, image deblurring and image subtraction, can be determined in terms of the output intensity distribution. For image deblurring the temporal coherence requirement depends on the ratio of the deblurring width to the smeared length of the blurred image. To obtain a higher degree of deblurring a narrower spectral width of the light source is required. For example, if the deblurring ratio $\Delta w/w$ is 0.1, the spectral width, $\Delta\lambda$, should be <640 Å.

For the spatial coherence requirement the image deblurring depends on both the deblurring ratio $\Delta w/w$ and the smeared length w. If the deblurring ratio $\Delta w/w = 1/10$ and w = 1 mm, a slit source <0.26 mm should be used. For a smeared image deblurring operation the constraints of the temporal and spatial coherence requirements are not critical, which can be achieved in practice.

For image subtraction, the temporal coherence requirement is determined by the highest spatial frequency and the separation of the input object transparencies. If the separation and spatial frequency of the input transparencies are high, a narrower spatial bandwidth of the light source is required.

For spatial coherence requirement, the modulation transfer function, which determines the contrast of the subtracted image, depends on the ratio of the slit width to the spatial period of the encoding mask, i.e., d/D. If the ratio d/D is low, a higher contrast subtracted image can be obtained. For example, with $d/D = 0.05$, a relatively higher MTF = 0.85 can be obtained. Compared with the image deblurring operations, the coherence requirements are more stringent for the subtraction process.

Finally, the solution to the coherence requirement for partially coherent processing is not restricted to the application of the deblurring and subtraction operation, but may also be applied to any other optical processing operation.

We wish to acknowledge the support by the U.S. Air Force Office of Scientific Research grant AFOSR-81-0148.

Appendix

To prove the following relationship:

$$\int_{-\infty}^{\infty} \frac{1}{\operatorname{sinc}\left(\frac{Wx}{\lambda_0 f}\right)} \exp\left(-j\frac{2\pi}{\lambda f}xu'\right) dx = -\left\{\frac{4f\lambda_0}{W}\sum_{n=1}^{\infty}(-1)^n \times \sin\frac{2\pi n\lambda_0}{\lambda W}u'\right\}\operatorname{sgn}(u'), \tag{A1}$$

we let $x/\lambda f = f_x$ and $\lambda/\lambda_0 W = l$.

The problem then reduces to finding the solution for

$$\lambda/l \int \frac{\pi fx}{\sin(\pi lfx)} \exp(j2\pi fxu')dfx. \quad \text{(A2)}$$

Since there are an infinite number of poles in the real domain, i.e.,

$$fx = n/l, \qquad n = 1,2,\ldots. \quad \text{(A3)}$$

Equation (A1) will be evaluated for the cases of $u' > 0$ and $u' \leq 0$. The contour integration, which is taken over the upper half of the complex plane (see Fig. 12), is given by

$$\left\{\int_{-\infty}^{\infty} - \Sigma \int_{f-\epsilon}^{f+\epsilon} + \int_R\right\} \frac{\pi fx}{\sin(\pi lfx)} \exp(-j2\pi fxu')dfx = 0, \quad \text{(A4)}$$

where x is the radius of the small half-circles around the poles, and R is the radius of the larger contour half-circle. Denote

$$z = R\exp(j\theta), \qquad dz = j\theta R\exp(j\theta)d\theta. \quad \text{(A5)}$$

The last term of Eq. (A4) may then be written

$$\int_R \frac{\pi fx}{\sin(\pi lfx)} \exp(j2\pi fxu')dfx = \int \frac{\pi z}{\sin(\pi lz)} \exp(j2\pi zu')dz$$
$$= \int_R \frac{-2\pi R^2 \exp(j2\pi Ru'\cos\theta)\exp(-2\pi R\sin\theta u')\theta\exp(2j\theta)}{\exp[j\pi lR(\cos\theta + j\sin\theta)] - \exp[-j\pi lR(\cos\theta + j\sin\theta)]} d\theta, \quad \text{(A6)}$$

so that

$$\lim_{R\to\infty} \int_R \frac{\pi fx}{\sin(\pi lfx)} \exp(j2\pi fxu')dfx = 0. \quad \text{(A7)}$$

But from Eq. (A4) it is easily shown that as R approaches infinity

$$\int_{-\infty}^{\infty} \frac{\pi fx}{\sin(\pi lfx)} \exp(j2\pi fxu')dfx = -2\pi j \sum_{n=-\infty}^{\infty} R_n, \quad \text{(A8)}$$

where

$$R_n = \lim_{z\to f}\left(z - \frac{n}{l}\right) \frac{\pi z\exp(j2\pi zu')}{\sin(\pi lz)} = \frac{(-1)^n n\exp(j2n\pi u'/l)}{\pi l^2}. \quad \text{(A9)}$$

Therefore,

$$\int_{-\infty}^{\infty} \frac{\pi fx}{\sin(\pi lfx)} \exp(j2\pi fxu')dfx = \frac{4}{l^2}\sum_{n=1}^{\infty} (-1)^n n \sin\frac{2\pi n}{l}u', \quad \text{for } u' > 0. \quad \text{(A10)}$$

The contour integral taken over the lower half of the plane as shown in Fig. 13 is similarly given by

$$\int_{-\infty}^{\infty} \frac{\pi fx}{\sin(\pi lfx)} \exp(j2\pi fxu')dfx = -\frac{4}{l^2}\sum_{n=1}^{\infty} (-1)^n n \sin\frac{2\pi n}{l}u', \quad \text{for } u' < 0. \quad \text{(A11)}$$

The results of Eqs. (A10) and (A11) thus prove that the equality of Eq. (A1) holds true.

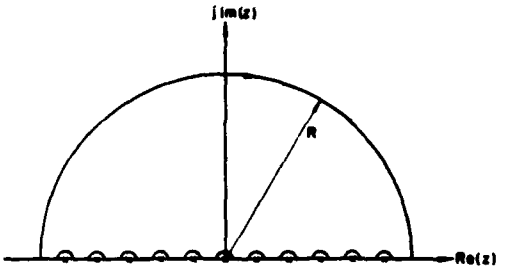

Fig. 12.

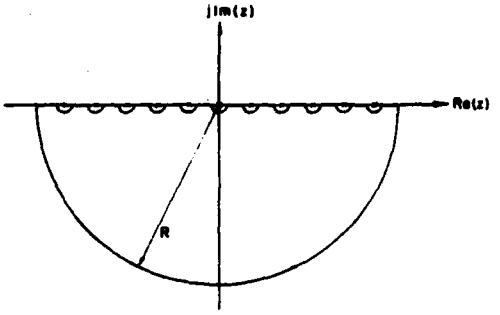

Fig. 13.

References

1. J. W. Goodman, *Introduction to Fourier Optics* (McGraw-Hill, New York, 1968).
2. F. T. S. Yu, *Introduction to Diffraction Information Processing and Holography* (MIT Press, Cambridge, 1973).
3. A. Vander Lugt, IEEE Proc. **62**, 1300 (1974).
4. G. L. Rogers, Opt. Laser Technol. **7**, 153 (1975).
5. M. A. Monahan. K. Bromley, and R. P. Bocker, Proc. IEEE **65**, 121 (1977).
6. K. Bromley, Opt. Acta. **21**, 35 (1974).
7. G. L. Rogers, *Noncoherent Optical Processing* (Wiley, New York, 1977).
8. S. Lowenthal and P. Chavel, in *Proceedings, ICO Jerusalem 1976 Conference on Holography and Optical Processing*, E. Marom, A. Friesem, and E. Wiener-Avnear, Eds. (Pergamon, New York, 1977).
9. A. Lohmann, Appl. Opt. **16**, 261 (1977).
10. E. N. Leith and J. Roth, Appl. Opt. **16**, 2565 (1977).
11. M. Born and E. Wolf, *Principles of Optics* (Pergamon, New York, 1970).
12. F. T. S. Yu, Opt. Comm. **27**, 23 (1978).
13. F. T. S. Yu, Appl. Opt. **17**, 3571 (1978).
14. F. T. S. Yu, Proc. Soc. Photo-Opt. Instrum. Eng. **232**, 9 (1980).
15. S. L. Zhuang, T. H. Chao, and F. T. S. Yu, Opt. Lett. **6**, 102 (1981).
16. K. Dutta and J. W. Goodman, J. Opt. Soc. Am. **67**, 796 (1977).
17. F. T. S. Yu, S. L. Zhuang, and S. T. Wu, Appl. Phys. **827**, 99 (1982).
18. S. T. Wu and F. T. S. Yu, Appl. Opt. **20**, 4082 (1981).

SECTION IV

Apparent Transfer Function

Appl. Phys. B 28, 359–366 (1982)

Applied Physics B Photophysics and Laser Chemistry

Apparent Transfer Function for Partially Coherent Optical Information Processing

S. L. Zhuang* and F. T. S. Yu

Electrical Engineering Department, The Pennsylvania State University
University Park, PA 16802, USA

Received 5 March 1982/Accepted 3 April 1982

Abstract. In this paper, the general formulations of the apparent transfer function for the partially coherent optical processor will be derived. Although these formulas show that the apparent transfer function is dependent upon the degree of spatial and temporal coherence, there is actually more variability in the spatial coherence. We note that the obtained formulas may also be used as a criterion in the selection of source size and spectral bandwidth of an incoherent light source. Thus a specific optical information processing operation can be carried out with an incoherent source.

PACS: 42.30, 42.80

The description of a transfer-function for a linear spatially invariant optical system is an important concept in image evaluation. The techniques of using amplitude and intensely sinusoidal objects as input signals to determine the transfer characteristic of a coherent and an incoherent optical system has been investigated previously [1, 2]. In the past, the concept of system transfer function has been used as a criterion to evaluate the image quality of an optical system.

However, a strict coherent or incoherent optical field is a mathematical idealization. An optical field that occurs in practice consists of a very limited degree of coherence, because the electromagnetic radiation from a real physical source is never strictly monochromatic. In reality, a physical source cannot be a point, but rather a finite extension which consists of many elementary radiators.

The optical system under the partially coherent regime has been studied by Becherer and Parrent [3], and Swing and Clay [4]. They have shown that there are difficulties in applying the linear system theory to the evaluation of imagery at high spatial frequencies. These difficulties are primarily due to the inapplicability of the linear system theory under partially coherence regime. Nevertheless, using a sinusoidal analysis, an apparent transfer function for a partially coherent optical system was obtained. The result is appreciably different from those that would have been obtained from a linear system concept, either in intensity or in complex amplitude. In a more recent paper, Dutta and Goodman [5] described a procedure for sampling the mutual intensity function so that the image of a partially coherent object can be reconstructed.

In this paper, we shall show that an apparent transfer function for an optical information processing system can be derived from a partially coherent illuminator. We shall show that the apparent transfer function of a partially coherent optical processor is dependent upon the temporal and spatial coherence of the light source. We shall also show that, the concept of transfer function is a valuable one that can be used as a criterion for selecting an appropriate incoherent light source for a specific information processing operation.

1. Apparent Transfer Function for Temporal Coherence

In a recent paper [6], we have evaluated the coherence requirement for a partially coherent optical information processing system. We have shown that the temporal and spatial coherence requirements are, re-

* Visiting scientist from Shanghai Optical Instrument Research Institute, Shanghai, China

0721-7269/82/0028/0359/$01.60

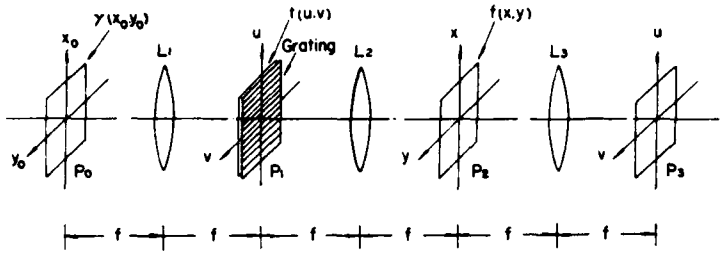

Fig. 1. A partially coherent optical information processor. (L: achromatic transform lans; p_0: source plane; p_1: input plane; p_2: spatial frequency plane; p_3: output plane)

spectively, dependent upon the spectral bandwidth and the source size of the light source. In the analysis of the temporal coherence requirement, we have assumed an infinitely small light source with finite spectral width. And for the evaluation of the spatial coherence requirement, we let monochromatic source with finite extent. In the evaluation of the apparent transfer for a partially coherent processing system, we shall also use these basic approaches.

We shall now evaluate the relationship between the apparent transfer function of an optical system and the spectral bandwidth of a light source. Let us now refer to the partially coherent optical information system of Fig. 1. We note that a diffraction grating is used at the input signal plane (u, v). The purpose of using a diffraction grating at the input plane is to disperse the input signal in the spatial frequency plane (x, y) so that a high spatial coherence can be achieved in the Fourier domain [7]. Thus the input signal can be processed in a complex amplitude, rather than in intensity, with a broad-band incoherent or white-light source. By using the partial coherent theory [8], we have computed a general output intensity distribution for the partially coherent processor, as shown in the following [7]:

$$I(u', v') = \int_{\lambda_0 - \Delta\lambda/2}^{\lambda_0 + \Delta\lambda/2} \iint_{-\infty}^{\infty} \gamma(x_0, y_0) s(\lambda) c(\lambda) \times \left| \iint_{-\infty}^{\infty} T(x_0 + x - \lambda f p_0, y_0 + y) f(x, y) e^{-j\frac{2\pi}{\lambda f}(xu' + yv')} dx dy \right|^2 \cdot dx_0 dy_0 d\lambda, \quad (1)$$

where λ_0 and $\Delta\lambda$ are the central wavelength and spectral width of the light source, $\gamma(x_0, y_0)$ is the source intensity distribution, $s(\lambda)$ and $c(\lambda)$ are the source spectral distribution and the spectral sensitivity of the recording material, respectively. $f(x, y)$ is the filter function at the Fourier plane, $T(x, y)$ is the Fourier spectrum of the input signal and p_0 is the spatial frequency of this diffraction grating. For simplicity, we assume that both $s(\lambda)$ and $c(\lambda)$ are constants which can be ignored in (1). We now use a sinusoidal input object transparency to evaluate the apparent transfer function of the optical processing system. The overall input signal transmittance, that includes the diffraction grating, can be written as:

$$t(u) = (1 + c\cos 2\pi\omega u)(1 + \cos 2\pi p_0 u), \quad (2)$$

where ω is the spatial frequency of sinusoidal signal and c is the contrast. For simplicity, we use a one dimension analysis. Thus, the output intensity distribution of Eq. (1) can be reduced to:

$$I(u', \Delta\lambda) = \int_{\lambda_0 - \Delta\lambda/2}^{\lambda_0 + \Delta\lambda/2} \int_{-\infty}^{\infty} \gamma(x_0) |A(x_0, u'; \lambda)|^2 dx_0 d\lambda, \quad (3)$$

where

$$A(x_0, u'; \lambda) = \int_{-\infty}^{\infty} T(x_0, x; \lambda) f(x) e^{-j\frac{2\pi}{\lambda f} xu'} dx. \quad (4)$$

is a complex amplitude function.

In order to achieve a higher temporal coherence requirement for the complex filtering process, we limit the spatial filter $f(x, y)$ to a finite extension in the x direction, i.e.,

$$f(x) = \text{rect}\left\{\frac{x - \lambda f p_0}{\Delta x}\right\}, \quad (5)$$

where Δx is the spatial width of the filter, and the filter is centered at $x = \lambda f p_0$ in the spatial frequency plane. Since the Fourier spectrum of the input signal at the spatial frequency plane p_2 is:

$$T(x_0, x; \lambda) = \int_{-\infty}^{\infty} (1 + c\cos 2\pi\omega u) \cdot (1 + \cos 2\pi p_0 u) e^{-j\frac{2\pi}{\lambda f} u(x_0 + x)} du \quad (6)$$

we obtain:

$$T(x_0, x; \lambda) = \delta\left(\frac{x_0 + x}{\lambda f}\right) + \frac{c}{2}\delta\left(\frac{x_0 + x}{\lambda f} - \omega\right) + \frac{c}{2}\delta\left(\frac{x_0 + x}{\lambda f} + \omega\right) + \frac{1}{2}\delta\left(\frac{x_0 + x}{\lambda f} - p_0\right) + \frac{1}{2}\delta\left(\frac{x_0 + x}{\lambda f} + p_0\right) + \frac{c}{4}\delta\left(\frac{x_0 + x}{\lambda f} - (\omega + p_0)\right) + \frac{c}{4}\delta\left(\frac{x_0 + x}{\lambda f} + (p_0 - \omega)\right)$$

$$+\frac{c}{4}\delta\left(\frac{x_0+x}{\lambda f}-(p_0-\omega)\right)+\frac{c}{4}\delta\left(\frac{x_0+x}{\lambda f}+(p_0+\omega)\right) \quad (7)$$

where $p_0 \gg \omega$.

In optical signal processing we focus only the first-order terms of (7) in the following

$$T(x_0,x;\lambda)=\frac{1}{2}\delta\left(\frac{x_0+x}{\lambda f}-p_0\right)+\frac{c}{4}\delta\left(\frac{x_0+x}{\lambda f}-(p_0-\omega)\right)+\frac{c}{4}\delta\left(\frac{x_0+x}{\lambda f}-(p_0+\omega)\right). \quad (8)$$

By substituting (5) and (8) into (4), we have:

$$\begin{aligned}A(x_0,u';\lambda)=&\int_{-\infty}^{\infty}\operatorname{rect}\left\{\frac{x-\lambda f p_0}{\Delta x}\right\}e^{-j\frac{2\pi}{\lambda f}xu'}dx\\&*\int_{-\infty}^{\infty}\frac{1}{2}\delta\left(\frac{x_0+x}{\lambda f}+p_0\right)e^{-j\frac{2\pi}{\lambda f}xu'}dx\\&+\int_{-\infty}^{\infty}\operatorname{rect}\left\{\frac{x-\lambda f p_0}{\Delta x}\right\}e^{-j\frac{2\pi}{\lambda f}xu'}dx\\&*\int_{-\infty}^{\infty}\frac{c}{4}\delta\left(\frac{x_0+x}{\lambda f}+p_0-\omega\right)e^{-j\frac{2\pi}{\lambda f}xu'}dx\\&+\int_{-\infty}^{\infty}\operatorname{rect}\left\{\frac{x-\lambda f p_0}{\lambda f}\right\}e^{-j\frac{2\pi}{\lambda f}xu'}dx\\&*\int_{-\infty}^{\infty}\frac{c}{4}\delta\left(\frac{x_0+x}{\lambda f}+p_0+\omega\right)e^{-j\frac{2\pi}{\lambda f}xu'}dx\\=&\left(\frac{1}{2}e^{j\frac{2\pi}{\lambda f}x_0u'}\operatorname{rect}\left\{\frac{x_0}{\Delta x}\right\}\right.\\&+\frac{c}{4}e^{j2\pi\left(\frac{x_0}{\lambda f}+\omega\right)u'}\operatorname{rect}\left\{\frac{x_0+\lambda f\omega}{\Delta x}\right\}\\&\left.+\frac{c}{4}e^{j2\pi\left(\frac{x_0}{\lambda f}-\omega\right)u'}\operatorname{rect}\left\{\frac{x_0-\lambda f\omega}{\Delta x}\right\}\right)e^{-j2\pi p_0u'},\end{aligned} \quad (9)$$

where $*$ denotes the convolution operation.

We now consider the effect due to temporal coherence. Let us now assume that the incoherent source is a point source, i.e., $\gamma(x_0)=\delta(x_0)$, thus (3) becomes

$$\begin{aligned}I(u',\Delta\lambda)=&\int_{\lambda_0-\Delta\lambda/2}^{\lambda_0+\Delta\lambda/2}A(u';\lambda)A^*(u';\lambda)d\lambda\\=&\int_{\lambda_0-\Delta\lambda/2}^{\lambda_0+\Delta\lambda/2}\left[\frac{1}{4}+\frac{c^2}{8}\operatorname{rect}\left\{\frac{\lambda f\omega}{\Delta x}\right\}\right.\\&+\frac{c}{2}\cos(2\pi\omega u')\operatorname{rect}\left\{\frac{\lambda f\omega}{\Delta x}\right\}\\&\left.+\frac{c^2}{8}\cos(2\pi(2\omega)u')\operatorname{rect}\left\{\frac{\lambda f\omega}{\Delta x}\right\}\right]d\lambda,\end{aligned} \quad (10)$$

where $\Delta\lambda$ is the spatial bandwidth of the light source. In the following, we shall attempt to evaluate the output intensity distribution of (10) in the following separated cases:

(i) for $\omega<\dfrac{\Delta x}{(2\lambda_0+\Delta\lambda)f}$, the output intensity distribution of Eq. (10) becomes

$$I^{(1)}(u',\Delta\lambda)=\left[\frac{1}{4}+\frac{c^2}{8}+\frac{c}{2}\cos(2\pi\omega u')+\frac{c^2}{8}\cos(2\pi 2\omega u')\right]\Delta\lambda, \quad (11)$$

where the image contrast for both basic and second harmonic frequencies are

$$\gamma_1^{(1)}(\omega)=\frac{4c}{2+c^2}, \quad (12a)$$

and

$$\gamma_2^{(1)}(\omega)=\frac{c^2}{2+c^2}; \quad (12b)$$

(ii) for $\dfrac{\Delta x}{f(2\lambda_0+\Delta\lambda)}<\omega<\dfrac{\Delta x}{f(2\lambda_0-\Delta\lambda)}$, we obtain

$$\begin{aligned}I^{(2)}(u',\Delta\lambda)=&\frac{1}{4}\Delta\lambda+\frac{c^2}{8}\left(\frac{\Delta x}{2f\omega}-\lambda_0+\frac{\Delta\lambda}{2}\right)\\&+\frac{c}{2}\cos(2\pi\omega u')\left(\frac{\Delta x}{2f\omega}-\lambda_0+\frac{\Delta\lambda}{2}\right)\\&+\frac{c^2}{8}\cos(2\pi 2\omega u')\left(\frac{\Delta x}{2f\omega}-\lambda_0+\frac{\Delta\lambda}{2}\right),\end{aligned} \quad (13)$$

and

$$\gamma_1^{(2)}(\omega)=\frac{4c(\Delta x-2f\omega\lambda_0+f\omega\Delta\lambda)}{4f\omega\Delta\lambda+c^2(\Delta x-2f\omega\lambda_0+f\omega\Delta\lambda)}, \quad (14a)$$

$$\gamma_2^{(2)}(\omega)=\frac{c^2(\Delta x-2f\omega\lambda_0+f\omega\Delta\lambda)}{4f\omega\Delta\lambda+c^2(\Delta x-2f\omega\lambda_0+f\omega\Delta\lambda)}; \quad (14b)$$

(iii) for $\omega>\dfrac{\Delta x}{f(2\lambda_0-\Delta\lambda)}$, (10) becomes

$$I^{(3)}(u',\Delta\lambda)=\frac{1}{4}\Delta\lambda. \quad (15)$$

and

$$\gamma_1^{(3)}(\omega)=\gamma_2^{(3)}(\omega)=0. \quad (16)$$

We also note that for the case of monochromatic point source, the output irradiance distribution is

$$I(u)=1+\frac{c^2}{2}+2c\cos(2\pi\omega u)+\frac{c^2}{2}\cos(2\pi 2\omega u'), \quad (17)$$

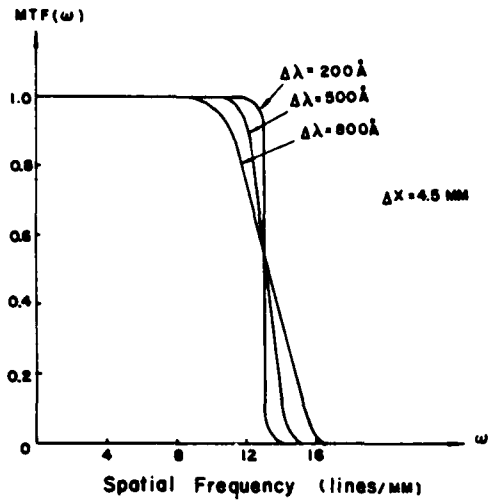

Fig. 2. Temporal coherence apparent transfer function as a function of input signal frequency ω, for various values of spectral width $\Delta\lambda$

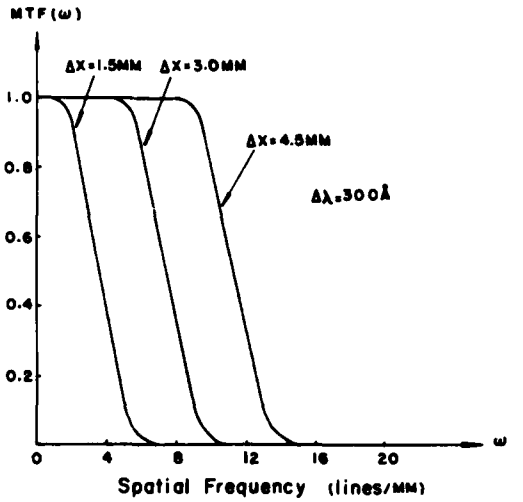

Fig. 3. Temporal coherence apparent transfer function as a function of ω, for various of spatial width of filter Δx

where

$$\gamma_1^{(0)} = \frac{4c}{2+c^2}, \tag{18a}$$

and

$$\gamma_2^{(0)} = \frac{c^2}{2+c^2}. \tag{18b}$$

Because the apparent transfer function can be obtained by the ratio of the contrast of the output basic frequency signal to the contrast of the input signal, we have

$$\mathrm{MTF}(\omega) = \begin{cases} 1 & \text{for } \omega < \dfrac{\Delta x}{f(2\lambda_0 + \Delta\lambda)} \\ \dfrac{(2+c^2)(\Delta x - 2f\omega\lambda_0 + f\omega\Delta\lambda)}{4f\omega\Delta\lambda + c^2(\Delta x - 2f\omega\lambda_0 + f\omega\Delta\lambda)} & \text{for } \dfrac{\Delta x}{f(2\lambda_0+\Delta\lambda)} \leqq \omega < \dfrac{\Delta x}{f(2\lambda_0-\Delta\lambda)} \\ 0 & \text{for } \omega \geqq \dfrac{\Delta x}{f(2\lambda_0-\Delta\lambda)} \end{cases} \tag{19}$$

which is depending upon the spatial frequency of the diffraction grating p_0, the spatial width of the filter Δx, and the spectral bandwidth of the light source $\Delta\lambda$.

We note that the width of the filter Δx should be chosen to coincide with the product of the spatial frequency p_0 of the diffraction grating, the focal length of the achromatic transform lens, and the spectral width $\Delta\lambda$ of the light source, i.e.,

$$\Delta x = p_0 f \Delta\lambda. \tag{20}$$

By substituting this relationship of (20) into (19), we have

$$\mathrm{MFT}(\omega) = \begin{cases} 1 & \text{for } \omega < \dfrac{p_0\Delta\lambda}{2\lambda_0 + \Delta\lambda} \\ \dfrac{(2+c^2)(p_0\Delta\lambda - 2\omega\lambda_0 + \omega\Delta\lambda)}{4\omega\Delta\lambda + c^2(p_0\Delta\lambda - 2\omega\lambda_0 + \omega\Delta\lambda)} & \text{for } \dfrac{p_0\lambda}{2\lambda_0+\Delta\lambda} \leqq \omega < \dfrac{p_0\lambda}{2\lambda_0-\Delta\lambda} \\ 0 & \text{for } \omega \geqq \dfrac{p_0\lambda}{2\lambda_0-\Delta\lambda}. \end{cases} \tag{21}$$

Which apparent transfer function reduces to a function of p_0 and $\Delta\lambda$.

We now illustrate the dependency of the apparent transfer function upon the spectral width of the light source $\Delta\lambda$, the spatial width of the filter Δx, and the spatial frequency of the grating p_0. Figure 2 shows the plots of the apparent transfer function (MTF) as a function of the input signal frequency ω for various values of spectral bandwidth $\Delta\lambda$. From this figure we notice that the MTF is not appreciably affected by the spectral bandwidth $\Delta\lambda$ of the light source, except for some slight changes in frequency response. For example, an $\Delta\lambda$ becomes broader, a slight reduction in lower frequency response is expected. However, the system bandwidth is somewhat slightly broader. Figure 3 shows the variation of MTF as a function of ω for various values of spatial width Δx of the filter and a

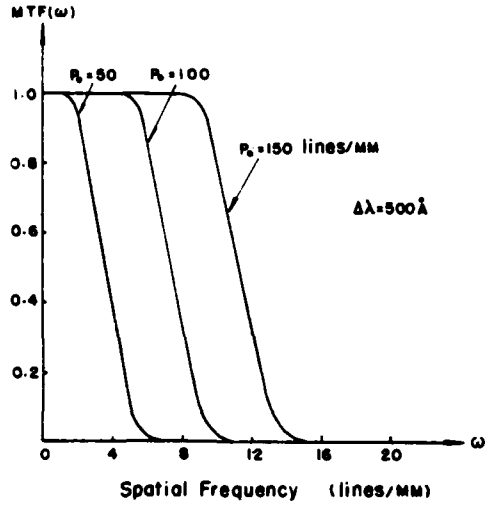

Fig. 4. Temporal coherence apparent transfer function as a function of ω, for various values of grating spatial frequency p_0

given $\Delta\lambda$. From this figure we see that the system bandwidth is linearly related to that of the spatial width of the filter. In other words, the larger the spatial width of the filter used, the wider the system bandwidth which may result. Figure 4 also shows the dependent of the MTF upon the spatial frequency of the grating p_0. Again, we see that the system bandwidth is linearly proportional to p_0, as expected from the relationship of (20). In other words, a higher frequency grating has the advantage of achieving finer image resolution. However, this advantage of using a higher spatial frequency grating is somewhat compensated with the use of a larger achromatic transform lens, to which is generally more expensive.

2. Apparent Transfer Function for Spatial Coherence

Now we shall determine the dependent of the apparent transfer function upon the source size Δs. To simplify our analysis, we assume that the light source is monochromatic but with finite extent. The output intensity distribution of (3) can therefore be written as:

$$I(u', \Delta s) = \int_{-\infty}^{\infty} \gamma(x_0) |A(u', x_0)|^2 dx_0 . \tag{22}$$

For simplicity, we assume that a uniform irradiance distribution of the extended light source exists, i.e.,

$$\gamma(x_0) = \text{rect}\left\{\frac{x_0}{\Delta s}\right\}, \tag{23}$$

where Δs is the extended source size with reference to (4), we see that

$$\begin{aligned} A(u', x_0)A^*(u', x_0) &= \frac{1}{4}\text{rect}\left\{\frac{x_0}{\Delta x}\right\} \\ &+ \frac{c^2}{16}\left(\text{rect}\left\{\frac{x_0+\lambda f\omega}{\Delta x}\right\} + \text{rect}\left\{\frac{x_0-\lambda_0 f\omega}{\Delta x}\right\}\right) \\ &+ \frac{c}{4}\cos(2\pi\omega u')\left(\text{rect}\left\{\frac{x_0+\frac{1}{2}\lambda_0 f\omega}{\Delta x-\lambda_0 f\omega}\right\}\right. \\ &\left. + \text{rect}\left\{\frac{x_0-\frac{1}{2}\lambda_0 f\omega}{\Delta x-\lambda_0 f\omega}\right\}\right) \\ &+ \frac{c^2}{8}\cos(2\pi 2\omega u')\,\text{rect}\left\{\frac{x_0}{\Delta x-2\lambda_0 f\omega}\right\}, \end{aligned} \tag{24}$$

where we have used the following relationship

$$\text{rect}\left\{\frac{x}{a}\right\}\text{rect}\left\{\frac{x+b}{a}\right\} = \text{rect}\left\{\frac{x+b/2}{a+b}\right\}. \tag{25}$$

By properly shifting the coordinate axis, (24) can be written as

$$\begin{aligned} A(u', x_0)A^*(u', x_0) &= \frac{1}{4}\text{rect}\left\{\frac{x_0}{\Delta x}\right\} \\ &+ \frac{c^2}{16}\left(\text{rect}\left\{\frac{x_0}{\Delta x+2\lambda_0 f\omega}\right\} + \text{rect}\left\{\frac{x_0}{\Delta x-2\lambda_0 f\omega}\right\}\right) \\ &+ \frac{c}{4}\cos(2\pi\omega u')\left(\text{rect}\left\{\frac{x_0}{\Delta x}\right\} + \text{rect}\left\{\frac{x_0}{\Delta x-2\lambda_0 f\omega}\right\}\right) \\ &+ \frac{c^2}{8}\cos(2\pi 2\omega u')\,\text{rect}\left\{\frac{x_0}{\Delta x-2\lambda_0 f\omega}\right\}. \end{aligned} \tag{26}$$

By substituting (23) and (26) into (22), we obtained the following output intensity distribution and the basic and second harmonic frequencies

(i) for $0 < \Delta s < \Delta x - 2\lambda_0 f\omega$, we have:

$$I^{(1)}(u', \Delta s) = \left[\left(\frac{1}{4} + \frac{c^2}{8}\right) + \frac{c}{2}\cos(2\pi\omega u') + \frac{c^2}{8}\cos(2\pi 2\omega u')\right]\Delta s, \tag{27}$$

and

$$\gamma_1^{(1)}(\omega) = \frac{4c}{2+c^2}, \tag{28a}$$

$$\gamma_1^{(2)}(\omega) = \frac{c^2}{2+c^2}; \tag{28b}$$

(ii) for $\Delta x - 2\lambda_0 f\omega < \Delta s < \Delta x$, we obtain

$$\begin{aligned} I^{(2)}(u', \Delta s) &= \left[\left(\frac{1}{4} + \frac{c^2}{16}\right)\Delta s + \frac{c^2}{16}(\Delta x - 2\lambda_0 f\omega)\right] \\ &+ \frac{c}{4}(\Delta s + \Delta x - 2\lambda_0 f\omega)\cos(2\pi\omega u') \\ &+ \frac{c^2}{8}(\Delta x - 2\lambda_0 f\omega)\cos(2\pi 2\omega u'), \end{aligned} \tag{29}$$

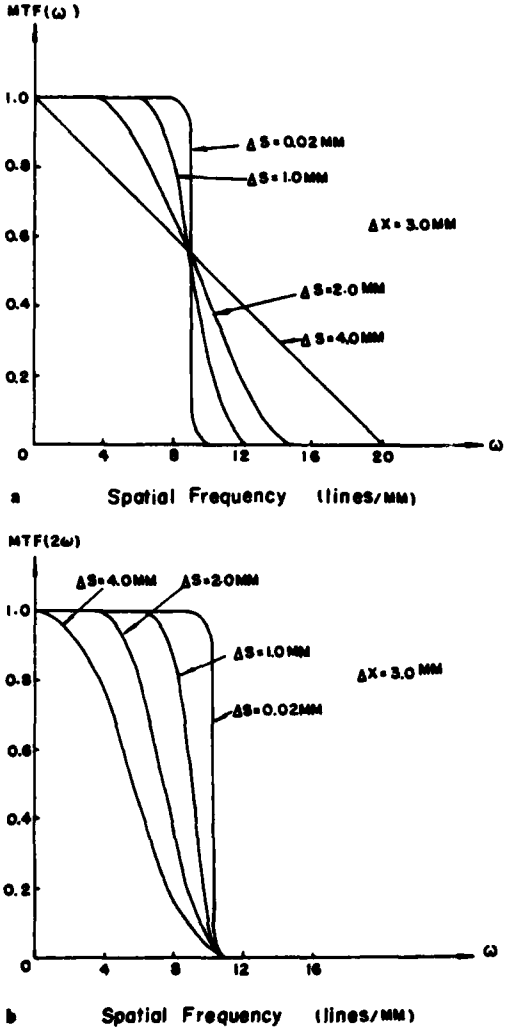

Fig. 5a and b. Spatial coherence apparent transfer function as a function of input signal frequency ω, for various values of source size Δs. (a) Basic MTF. (b) Second-harmonic MTF

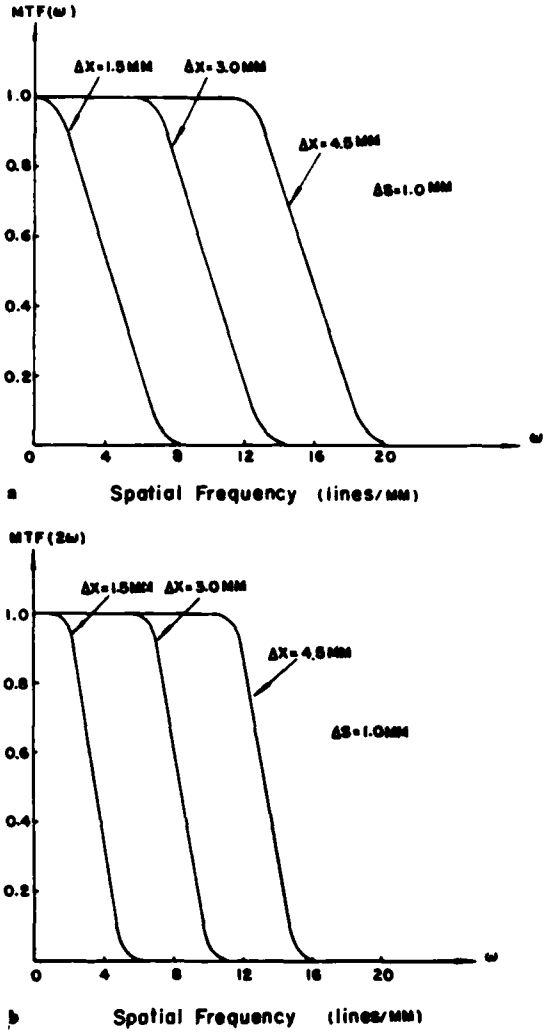

Fig. 6a and b. Spatial coherence apparent transfer function as a function of input signal frequency ω, for various values of filter width Δx. (a) Basic MTF. (b) Second harmonic MTF

and

$$\gamma_1^{(2)}(\omega)=\frac{4c(\Delta s+\Delta x-2\lambda_0 f\omega)}{4\Delta s+c^2(\Delta s+\Delta x-2\lambda_0 f\omega)}, \tag{30a}$$

$$\gamma_2^{(2)}(\omega)=\frac{2c^2(\Delta x-2\lambda_0 f\omega)}{4\Delta s+c^2(\Delta s+\Delta x-2\lambda_0 f\omega)}; \tag{30b}$$

(iii) for $\Delta x<\Delta s<\Delta x+2\lambda_0 f\omega$, (26) becomes

$$I^{(3)}(u',\Delta s)=\left(\frac{1}{4}+\frac{c^2}{16}\right)\Delta x+\frac{c^2}{16}(\Delta s-2\lambda_0 f\omega)+\frac{c}{2}(\Delta x-\lambda_0 f\omega)\cos(2\pi\omega u')+\frac{c^2}{8}(\Delta x-2\lambda_0 f\omega)\cos(2\pi 2\omega u'). \tag{31}$$

$$\gamma_1^{(3)}(\omega)=\frac{8c(\Delta x-\lambda_0 f\omega)}{4\Delta x+c^2(\Delta s+\Delta x-2\lambda_0 f\omega)}, \tag{32a}$$

and

$$\gamma_2^{(3)}(\omega)=\frac{2c^2(\Delta x-2\lambda_0 f\omega)}{4\Delta x+c^2(\Delta s+\Delta x-2\lambda_0 f\omega)}; \tag{32b}$$

(iv) for $\Delta s>\Delta x+2\lambda_0 f\omega$, we have:

$$I^{(4)}(u',\Delta s)=\left(\frac{1}{4}+\frac{c^2}{8}\right)\Delta x+\frac{c}{2}(\Delta x-\lambda_0 f\omega)\cos(2\pi\omega u')+\frac{c^2}{8}(\Delta x-2\lambda_0 f\omega)\cos(2\pi 2\omega u') \tag{33}$$

$$\gamma_1^{(4)}(\omega)=\frac{4c(\Delta x-\lambda_0 f\omega)}{(2+c^2)\Delta x}, \tag{34a}$$

and

$$\gamma_2^{(4)}(\omega)=\frac{c^2(\Delta x-2\lambda_0 f\omega)}{(2+c^2)\Delta x}\,; \tag{34b}$$

(c) for $\Delta x<\omega\lambda_0 f$, we again obtain

$$I^{(5)}(u',\Delta s)=\text{constant}. \tag{35}$$

and

$$\gamma_1^{(5)}(\omega)=\gamma_2^{(5)}(\omega)=0. \tag{36}$$

Notice that where this cut-off frequency of the optical system is $\omega_{max}=\Delta x/\lambda_0 f$. Thus the apparent transfer function of the optical processing system, for both the basic and second harmonic frequencies are

$$\mathrm{MTF}(\omega)=\begin{cases}1 & \text{for } 0\leqq\Delta s<\Delta x-2\lambda_0 f\omega\\ \dfrac{(2+c^2)(\Delta s+\Delta x-2\lambda_0 f\omega)}{4\Delta s+c^2(\Delta s+\Delta x-2\lambda_0 f\omega)} & \text{for } \Delta x-2\lambda_0 f\omega\leqq\Delta s<\Delta x\\ \dfrac{2(2+c^2)(\Delta x-\lambda_0 f\omega)}{4\Delta x+c^2(\Delta s+\Delta x-2\lambda_0 f\omega)} & \text{for } \Delta x\leqq\Delta s\leqq\Delta x+2\lambda_0 f\omega\\ \dfrac{\Delta x-\lambda_0 f\omega}{\Delta x} & \text{for } \Delta x+2\lambda_0 f\omega\leqq\Delta s\\ 0 & \text{for } \Delta x\leqq\omega\lambda_0 f\end{cases} \tag{37}$$

and similarly:

$$\mathrm{MTF}(2\omega)=\begin{cases}1 & \text{for } 0\leqq\Delta s<\Delta x-2\lambda_0 f\omega\\ \dfrac{2(2+c^2)(\Delta x-2\lambda_0 f\omega)}{4\Delta s+c^2(\Delta s+\Delta x-2\lambda_0 f\omega)} & \text{for } \Delta x-2\lambda_0 f\omega\leqq\Delta s<\Delta x\\ \dfrac{2(2+c^2)(\Delta x-2\lambda_0 f\omega)}{4\Delta x+c^2(\Delta s+\Delta x-2\lambda_0 f\omega)} & \text{for } \Delta x\leqq\Delta s<\Delta x+2\lambda_0 f\omega\\ \dfrac{\Delta x-2\lambda_0 f\omega}{\Delta x} & \text{for } \Delta x+2\lambda_0 f\omega\leqq\Delta s\\ 0 & \text{for } \Delta x\leqq\lambda_0 f\omega.\end{cases} \tag{38}$$

From the above equations, one may see that MTF, either for the fundamental or for the second-harmonic frequency, decreases rather rapidly as the source size Δs increases. Figure 5a shows MTF as a function of input spatial frequency ω, for various values of source size Δs. From this figure, we discover that the frequency response (i.e., MTF) decreases quite rapidly as the source size increases. In other words, for a fixed filter size, the smaller the source size used, the better the system frequency response. We also see that, where the source size is adequately small (e.g., $\Delta s\leqq 0.02$ mm) the MTF approaches the strict coherent MTF, on the other hand, if the source size is significantly large (e.g., $\Delta s\geqq 4$ mm) the MTF approaches that of the incoherent case. Figure 5b shows the second-harmonic MTF as a function of input spatial frequency ω. From the figure, we see that frequency response decreases even faster as the source size increases. Unlike the first harmonic MTF of Fig. 5a, the cut-off frequency tends to stay at the same values, although the higher frequency response decreases rather rapidly.

Figures 6a and 6b show the basic and the second-harmonic MTF as a function of input spatial frequency ω, for various sizes of spatial filters Δx, for a given Δs. From these two figures, again we see that the transfer system bandwidth is linearly related to the size of the spatial filter. Thus MTF is obviously limited by the filter bandwidth of the optical processor. The increase of filter bandwidth also causes a reduction in temporal coherence, which in turn reduces the processing capability. Nevertheless, an optimum processing capability can be obtained with the appropriate MTF for certain optical processing operations.

3. Conclusion

The nonlinear behavior of the partially coherent optical processor, when considering either intensity or amplitude distribution input signals, necessitates the use of the apparent transfer function to accurately predict the system response. We have derived the general formulas for MTF in terms of the theory of partially coherent light. These derivations indicate the dependence of MTF upon the degree of spatial coherence (i.e., the source size) as well as the degree of temporal coherence (i.e., the source spectral bandwidth). MTF has been shown to be less dependent

upon the spatial coherence requirement as compared to its relationship with the temporal coherence requirement.

It has been noted that the spatial bandwidth of our optical processor is primarily dependent upon the size of the filter Δx, where the filter is placed in the Fourier plane. The transfer systems bandwidth may be increased by using a larger spatial filter Δx. However, the size of the filter is selected such that $\Delta x = p_0 f \Delta\lambda$, which is linearly related to the spatial frequency of grating, the focal length of the transform lens and the spectral width of the light source. A narrow spectral band $\Delta\lambda$ is necessary for most partially coherent optical information processing operations. In order to achieve the required $\Delta\lambda$ for a wide strip of spatial filter Δx in the spatial frequency plane, a diffraction grating of sufficiently high frequency p_0 at the input plane is needed. For example, for partially coherent processing with a white light source, a set of narrow spectral band filters, each with a spectral bandwidth $\Delta\lambda$, can be used in the spatial frequency plane. Finally, we stress that the apparent transfer function which we have obtained is rather general and may be applied to any partially coherent optical processing system.

Acknowledgement. This work is supported by U.S. Air Force Office of Scientific Research under grant no. AFOSR-81-0148.

References

1. E.L. O'Neill: *Introduction to Statistical Optics* (Addison-Wesley, Reading, MA 1963)
2. J.W. Goodman: *Introduction to Fourier Optics* (McGraw-Hill, New York, NY 1968)
3. R.J. Becherer, G.B. Parrent: J. Opt. Soc. Am. **57**, 1479–1486 (1967)
4. R.E. Swing, J.R. Clay: J. Opt. Soc. Am. **57**, 1180–1189 (1967)
5. K. Dutta, J.W. Goodman: J. Opt. Soc. Am. **67**, 796–802 (1977)
6. F.T.S. Yu: Opt. Commun. **27**, 23–26 (1978)
7. S.L. Zhuang, F.T.S. Yu: "Coherence Requirement for Partially Coherent Optical Processing", Appl. Opt. (to be published)
8. M. Born, E. Wolf: *Principles of Optics*, 4th ed. (Pergamon Press, New York, NY 1970)

SECTION V

Source Encoding and Signal Sampling

SOURCE ENCODING, SIGNAL SAMPLING AND FILTERING FOR WHITE-LIGHT SIGNAL PROCESSING

by F. T. S. Yu

Electrical Engineering Department, The Pennsylvania State University
University Park, Pennsylvania 16802

Abstract

A relation between spatial coherence and source encoding intensity distribution is presented. Since the spatial coherence requirement is determined by the signal processing operation, a strict coherence source may not be needed for the processing. The advantage of the source encoding is to relax the constraints of strict spatial coherence requirement so that the signal processing operation can be carried out with an extended incoherent source. The effects of signal sampling on coherence requirement is discussed. The advantage of signal sampling is to improve the degree of temporal coherence in the Fourier plane so that the signal can be processed in complex amplitude with a broadband white-light source. Finally, experimental demonstrations are included.

Introduction

Since the invention of laser (i.e., a strong coherent source), laser has become a fashionable tool for many scientific applications particularly as applied to coherent optical signal processing. However coherent optical signal processing systems are plagued with coherent noises, which frequently limit their processing capability. As noted by the late Gabor, the Nobel prize winner in physics in 1970 for his invention of holography, the coherent noise is the number one enemy of the Modern Optical Signal Processing[1]. Aside the coherent noise, the coherent sources are usually expensive, and the coherent processing environments are very stringent. For example, heavy optical benches and dust free environments are generally required.

Recently, we have looked at the optical processing from a different standpoint. A question arises, is it necessarily true that all optical signal processing required a coherent source? The answer to this question is that there are many optical signal processings that can be carried out by a white-light source[2]. The advantages of the proposed white-light signal processing technique are: 1. It is capable of suppressing the coherent noise; 2. White-light sources are usually inexpensive; 3. The processing environments are not critical; 4. The white-light system is relatively easy and economical to maintain; and 5. The white-light processor is particularly suitable for color image processing.

One question that the reader may ask, since the white-light system offers all these glamorous merits, why it has been ignored for so long? The answer to this question is that, it was a general acceptance that an incoherent source cannot process the signal in complex amplitude. However, none of the practical sources are strictly incoherent, even a white-light source. In fact, we were able to utilize the partial coherence of a white-light source to perform the complex amplitude processing. The proposed white-light processor, on one hand it is capable of suppressing the coherent noise like an incoherent processor, on the other hand it is capable of processing the signal in complex amplitude like a coherent processor.

There is however a basic different approach toward a coherent and a white-light processor. In coherent processing, virtually no one seems to care about the coherence requirements, since the laser provides a strong coherent source. However, in white-light processing, the knowledge of the coherence requirement is usually needed.

In white-light processing we would approach the problem backward. First, we should know what is the processing operation we wish to perform: Is it a 1-D or 2-D processing? Is the signal filtering a point or point-pair concept? What is the spatial bandwidth of the signal? etc. Then with this knowledge, we would be able to evaluate the coherence requirements at the Fourier and at the input planes. From the evaluated results, we would be able to design a signal sampling function and a source encoding function to obtain these requirements. The objective of using a signal sampling function is to achieve a high degree of temporal coherence in Fourier plane so that the signal can be processing in complex amplitude, for the entire spectral band of a white-light source. And for the source encoding is to alleviate the constraints of an extended white-light source.

In the following sections, we shall discuss in detail the source encoding, signal sampling

CH1880-4/83/0000/0111$01.00 © 1983 IEEE

and filtering as applied to a white-light signal processing.

White Light Signal Processing

We shall now describe an optical signal processing technique that can be carried out by a white-light source, as illustrated in Fig. 1. The white-light signal processing system is similar to that of a coherent system, except the use of a white-light source, source encoding mask, signal sampling grating, and achromatic transform lenses. For example, if we place a signal transparency $s(x,y)$ in contact with a sampling phase grating, the complex light field for every wavelength λ behind the achromatic transform lens L_1 would be

$$E(p,q;\lambda) = \iint s(x,y)\exp(ip_o x)\exp[-i(px+qy)]dxdy$$

$$= S(p-p_o,q), \qquad (1)$$

where the integral is over the spatial domain of the input plane P_1, (p,q) denotes the angular spatial frequency coordinate system, p_o is the angular spatial frequency of the sampling phase grating, and $S(p,q)$ is the Fourier spectrum of $s(x,y)$. If we write Eq. (1) in the form of linear spatial coordinate system (α,β), we have,

$$E(\alpha,\beta;\lambda) = S(\alpha - \frac{\lambda f}{2\pi} p_o, \beta), \qquad (2)$$

where $p \triangleq (2\pi/\lambda f)\alpha$, $q \triangleq (2\pi/\lambda f)\beta$, and f is the focal length of the achromatic transform lens. Thus, we see that the Fourier spectra would disperse into rainbow color along the α axis, and each Fourier spectrum for a given wavelength λ is centered at $\alpha \pm (\lambda f/2\pi)p_o$.

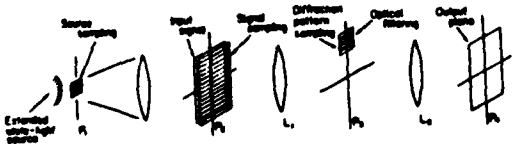

Fig. 1. A white-light optical signal processor.

In signal filtering, we assume that a sequence of complex spatial filters for various λ_n are available, i.e., $H(p_n,q_n)$, where $p_n = (2\pi/\lambda_n f)\alpha$, $q_n = (2\pi/\lambda_n f)\beta$. In practice, all the processing signals are spatial frequency limited, the spatial bandwidth of each $H(p_n,q_n)$ is also bandlimited, such as

$$H(p_n,q_n) = \begin{cases} H(p_n,q_n), & \alpha_1 < \alpha < \alpha_2, \\ 0, & \text{otherwise}, \end{cases} \qquad (3)$$

where $\alpha_1 \triangleq (\lambda_n f/2\pi)(p_o + \Delta p)$ and $\alpha_2 = (\lambda_n f/2\pi)(p_o - \Delta p)$ are the upper and the lower spatial limits of $H(p_n,q_n)$, and Δp is the spatial bandwidth of the input signal $s(x,y)$.

The limiting wavelengths of each $H(p_n,q_n)$ can be written as

$$\lambda_\ell = \lambda_n \frac{p_o + \Delta p}{p_o - \Delta p}, \text{ and } \lambda_h = \lambda_n \frac{p_o - \Delta p}{p_o + \Delta p}. \qquad (4)$$

The spectral bandwidth of $H(p_n,q_n)$ is therefore,

$$\Delta\lambda_n = \lambda_n \frac{4p_o\Delta p}{p^2 - (\Delta p)^2} \simeq \frac{4\Delta p}{p_o}\lambda_n. \qquad (5)$$

If we place this set of spatial filters side-by-side positioned over the smeared Fourier spectra, then the intensity distribution of the output light field can be shown as,

$$I(x,y) \simeq \sum_{n=1}^{N} \Delta\lambda_n \left|s(x,y;\lambda_n)*h(x,y;\lambda_n)\right|^2, \qquad (6)$$

where $h(x,y;\lambda)$ is the spatial impulse response of $H(p_n,q_n)$ and * denotes the convolution operation. Thus, the proposed white-light signal processor is capable of processing the signal in complex amplitude. Since the output intensity is the sum of the mutually incoherent narrow band irradiances, the annoying coherent noise can be eliminated. Furthermore, the white-light source contains all the color wavelengths, the proposed system is particularly suitable for color signal processing.

Spatial Filtering, Signal Sampling and Source Encoding

We have mentioned earlier for white-light processing, we would approach the problem in backward manner. For example, if signal filtering is two-dimensional (e.g., 2-D correlation operation), we would synthesize a set of narrow spectral band filters for each λ_n for the entire smeared Fourier spectra, as illustrated in Fig. 2(a). On the other hand, if the signal filtering is one-dimensional (e.g., deblurring due to linear motion), a broadband fan-shape spatial filter, to accomodate the scale variation due to wavelength, can be utilized as illustrated in Fig. 2(b). Since the filtering is taken place with the entire spectral band of the light source, the coherent noise can be suppressed and the white-light processing technique is very suitable for color image processing.

There is, however, a temporal coherence requirement imposed upon the signal filtering in Fourier plane. Since the scale of the Fourier spectrum varies with wavelength, a temporal coherence requirement should be imposed on each spatial filter at the Fourier plane. Thus, the spectral spread over each filter $H(p_n,q_n)$ is imposed by the temporal coherence requirement, i.e.,

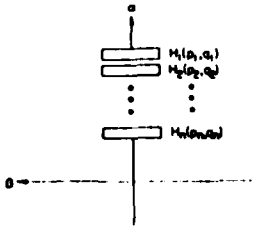

(a) A multi-spectral-band filter.

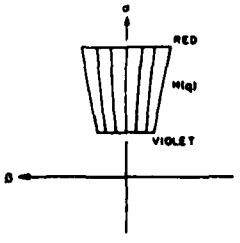

(b) A fan-shape filter

Fig. 2.

$$\frac{\Delta\lambda_n}{\lambda_n} \simeq \frac{4\Delta p}{p_o} << 1. \qquad (7)$$

From this requirement, a high degree of temporal coherence is achievable in the Fourier plane by simply increasing the spatial frequency of the sampling grating. Needless to say that, the same temporal coherence requirement of Eq. (7) can also be applied for a broadband fan-shape filter.

There is also a spatial coherence requirement imposed at the input plane of the white-light processor. With reference to the Wolf's partial coherence theory[3], the spatial coherence function at the input plane can be shown[4].

$$\Gamma(\vec{x}-\vec{x}') = \iint \gamma(\vec{x}_o)\exp[i2\pi \frac{\vec{x}_o}{\lambda f}(\vec{x}-\vec{x}')]d\vec{x}_o, \qquad (8)$$

where $\gamma(\vec{x}_o)$ denotes the intensity distribution of the source encoding function.

From the above equation, we see that the spatial coherence and source encoding function form a Fourier transform pair, i.e.,

$$\gamma(\vec{x}_o) = \mathcal{F}[\Gamma(\vec{x}-\vec{x}')], \qquad (9)$$

and

$$\Gamma(\vec{x}-\vec{x}') = \mathcal{F}^{-1}[\gamma(\vec{x}_o)], \qquad (10)$$

where $\mathcal{F}$ denotes the Fourier transformation. This Fourier transform pair implies that if a spatial coherence function is given then the source encoding function can be evaluated through the Fourier transformation and vice versa. We note that the source encoding function can consist of apertures of any shape or complicated gray scale transparency. However the source encoding function is only limited to a positive real quantity which is restricted by the following physical realizable condition:

$$0 \le \gamma(\vec{x}_o) \le 1. \qquad (11)$$

In white-light processing, we would search for a reduced spatial coherence requirement for the processing operation. With reference to this reduced spatial coherence function, a source encoding function that satisfied the physical realizability condition ca.. be obtained. One of the basic objectives of the source encoding is to alleviate the constraint of a white-light source. Furthermore the source encoding also improves the utilization of the light source such that the optical processing can be carried out by an extended source.

We shall now illustrate an application of the source encoding, signal sampling and filtering for a white-light signal processing. Let us now consider a polychromatic image subtraction[5]. The image subtraction of Lee[6] that we would consider is essentially a one-dimensional processing operation, in which a 1-D fan-shape diffraction grating should be utilized, as illustrated in Fig. 3. We note that the fan-shape grating (i.e., filter) is imposed by the temporal coherence condition of Eq. (7). Since the image subtraction is a point-pair processing operation, a strictly broad spatial coherence function at the input plane is not required. In other words, if one maintains the spatial coherence between the corresponding image points to be subtracted at the input plane, then the subtraction operation can be carried out at the output image plane. Thus instead of using a strictly broad spatial coherence function, a reduced spatial coherence function may be utilized, such as

$$\Gamma(y-y') = \delta(y-y'-h_o) + \delta(y-y'+h_o), \qquad (12)$$

where $2h_o$ is the main separation between the two input color transparencies. The source encoding function can therefore be evaluated by through the Fourier transform of Eq. (9), such as

$$\gamma(y_o) = 2\cos(\frac{2\pi h_o}{\lambda f} y_o). \qquad (13)$$

Unfortunately Eq. (13) is a bipolar function which is not physically realizable. To ensure a physically realizable source encoding function, we let a reduced spatial coherence function with the required point-pair coherence characteristic be:

$$\Gamma(|y-y'|) = \frac{\sin(\frac{N\pi}{h_o}|y-y'|)}{N\sin(\frac{\pi}{h_o}|y-y'|)} \operatorname{sinc}(\frac{\pi w}{h_o d}|y-y'|), \qquad (14)$$

where $N >> 1$ a positive integer, and $w << d$. Equation (14) represents a sequence of narrow

pulses which occur at every $|y-y'| = nh_o$, where n is a positive integer, and their peak values are weighted by a broader sine factor, as shown in Fig. 4(a). Thus, a high degree of spatial coherence can be achieved at every point-pair between the two input color transparencies. By taking the Fourier transformation of the reduced spatial coherence function of Eq. (14), the corresponding source encoding function is

$$\gamma(|y|) = \sum_{n=1}^{N} \text{rect}\,\frac{|y-nd|}{w}, \qquad (15)$$

where w is the slit width, $d = (\lambda f/h_o)$ is the separation between the slits, and N is the number of the slits. Since $\gamma(|y|)$ is a positive real function which satisfies the constraint of Eq. (11), the proposed source encoding function of Eq. (15) is physically realizable.

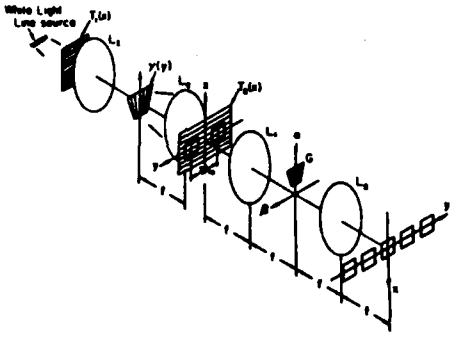

Fig. 3. A white-light image subtraction processor. T(x); phase grating, L_I; image lens, L_C; collimated lens, L_1 and L_2; achromatic transform lenses, γ(y); source encoding mask, G; fan-shape diffraction grating.

In view of Eq. (15), we also note that, the separation of slit d is linearly proportional of the λ. The source encoding is a fan-shape type function, as shown in Fig. 4(b). To obtain lines of rainbow color spectral light source for the signal processing, we would utilize a linear extended white-light source with a dispersive phase grating, as illustrated in Fig. 3. Thus with appropriate source encoding, signal sampling and filtering, color image subtraction operation can be obtained at the output plane. We stress again, the basic advantage of source encoding is to alleviate the constraint of strict spatial coherence requirement imposed upon the optical signal processor. The source encoding also offers the advantage of efficient utilization of the light power.

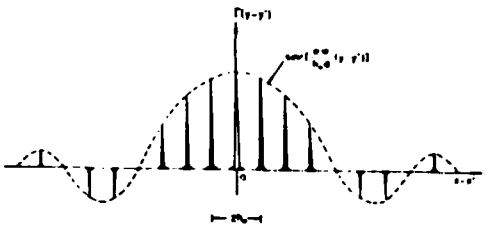

(a) A spatial coherence function.

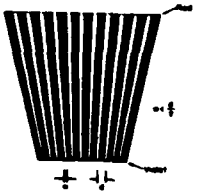

(b) A source encoding mask.

Fig. 4.

Experimental Demonstrations

We shall now provide a couple of experimental results obtained with the source encoding, signal sampling and filtering technique for white-light and extended incoherent sources. We shall first show the result obtained for color image deblurring due to linear motion with the white-light processing technique. Since linear motion deblurring is a 1-D processing operation and the inverse filtering is a point-by-point filtering concept such that the operation is taking place on the smearing length of the blurred image. Thus the deblurring filter (i.e., inverse filter) is a fan-shape type spatial filter[8] and the temporal coherence requirement is imposed by Eq. (11). The spatial coherence requirement is dependent upon the smearing length. A source encoding function of a narrow slit width (dependent upon the smearing) perpendicular to the smearing length is utilized. Figure 5(a) shows a black-and-white color picture of a blurred image due to linear motion of a F-16 fighter plane. The body of the fighter plane is painted in black-and-white colors, the wings are mostly painted in red, the tail is black-and-white, and the ground terrain is generally bluish color. From this figure, we see that the plane is badly blurred. Figure 5(b) shows the color image deblurringr result that we obtained with the proposed white-light deblurring technique. From this deblurred result, the letters and overall shape of the entire airplane are more distinctive than the blurred one. Furthermore, the river, the highways, and the

forestry of the ground terrain are far more visible. We note that the color reproduction of the deblurred image is spectacularly faithful, and coherent artifact noise is virtually non-existed. There is, however, some degree of color blur and color deviation, which are primarily due to the chromatic aberration and the anti-reflectance coating of the transform lenses. Nevertheless, these drawbacks can be overcome by utilizing good quality achromatic transform lenses.

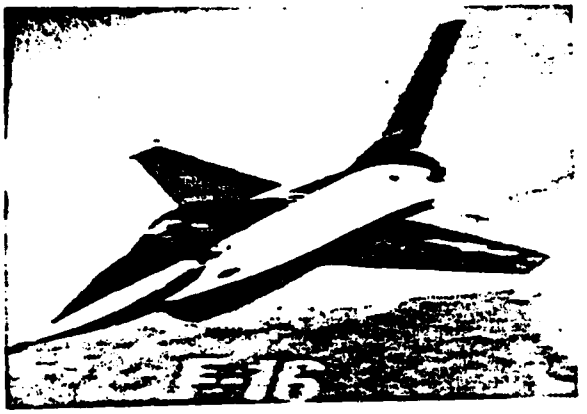

(a) A black-and-white picture of a blurred color image.

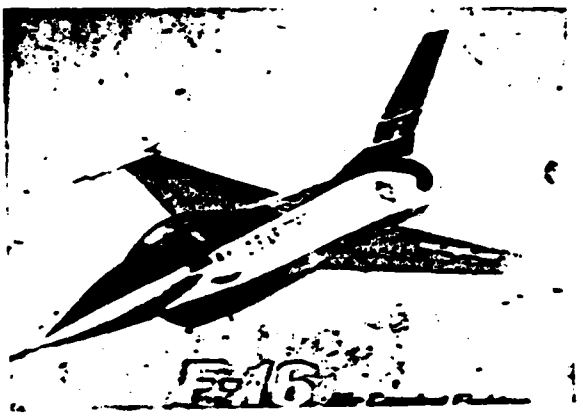

(b) A black-and-white picture of a deblurred color image.

Fig. 5.

Let us now provide a color image subtraction utilized by the source encoding technique with extended incoherent sources as described in previous sections. Figure 6(a) and 6(b) shows two black-and-white color image transparencies of a parking lot as input color objects. Figure 6(c) shows the color subtracted image obtained by the source encoding technique with extended incoherent source. In this figure, the profile of a (red) subcompact car can be seen at the output image plane. The shadow and the parking line (in yellow color) can also be readily identified. We however note that, this color image subtraction result is obtained by two narrow band extended incoherent sources. Extention toward the entire spectral band of a white-light source is currently under investigation.

(a) A black-and-white picture of the input color objects.

(b) A black-and-white picture of the input color objects.

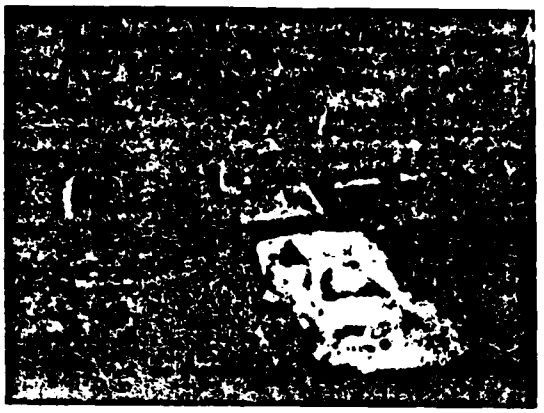

(c) A black-and-white picture of the subtracted color image.

Fig. 6.

Conclusion

In conclusion we would point out that the advantage of source encoding is to provide an appropriate spatial coherence function at the input plane so that the signal processing can be carried out by an extended incoherent source. The effect of the signal sampling is to achieve the temporal coherence requirement at the Fourier plane so that the signal can be processed in complex amplitude. If the filtering operation is two-dimensional, a multi-spectral-band 2-D filters should be utilized. If the filtering operation is one-dimensional, a fan-shape filter can be used.

In short, one should carry out the processing requirements backward for a white-light processing. With these processing requirements (e.g., operation, temporal and spatial coherence requirements), multi-spectral-band or broad-band filter, signal sampling function, and source encoding mask can be synthesized. Thus the signal processing can be carried out in complex amplitude over the whole-spectral band of the light source.

We acknowledge the support of the U.S. Air Force Office of Scientific Research Grant AFOSR-81-0148.

References

1. D. Gabor, IBM, J. Res. Develop, 14, 509 (1970).

2. F.T.S. Yu, Optical Information Processing, Wiley-Interscience, N[illegible], 1983.

3. M. Born and E. Wolf, Principles of Optics, 2nd rev. ed., Pergamon Press, New York, 1964.

4. F.T.S. Yu, S.L. Zhuang, and S.T. Wu, Appl. Phys., B27, 99 (1982).

5. F.T.S. Yu and S.T. Wu, J. Opt., 13, 183 (1982).

6. S.H. Lee, S.K. Yao, and A.G. Milns, J. Opt. Soc. Am., 60, 1037 (1970).

7. S.T. Wu and F.T.S. Yu, Appl. Opt., 20, 4082 (1981).

8. T.H. Chao, S.L. Zhuang, S.Z. Mao and F.T.S. Yu, Appl. Opt., to be published.

SECTION VI

Color Image Subtraction

Original article

J. Optics (Paris), 1982, vol. *13*, n° 4. pp. 183-187

ELECTRICAL ENGINEERING DEPARTMENT
THE PENNSYLVANIA STATE UNIVERSITY

University Park, PA 16802 (U.S.A.)

COLOR IMAGE SUBTRACTION WITH EXTENDED INCOHERENT SOURCES

F. T. S. YU, S. T. WU (*)

MOTS CLÉS :

Soustraction d'images en couleur
Sources incohérentes codées

KEY WORDS :

Color image subtraction
Coded incoherent sources

Soustraction d'images en couleur utilisant des sources étendues incohérentes

SUMMARY : A technique of color image subtraction with encoded extended incoherent sources is presented. The objective of the source encoding is to obtain a reduced coherence requirement for the image subtraction so that the inherent difficulty of obtaining an incoherent point source can be alleviated. Experimental results for the color image subtraction obtained with the incoherent processing technique are given. Since most images are multi-colored, this color image subtraction technique may offer a broad range of applications.

RÉSUMÉ : Nous présentons une méthode de soustraction d'images en couleur utilisant des sources incohérentes codées. Le but du codage est d'obtenir la cohérence nécessaire pour notre expérience avec une source relativement grande. Nous donnons des résultats expérimentaux. La plupart des images étant des images en couleur, cette technique de soustraction peut avoir des applications diverses.

I. — *INTRODUCTION*

One of the most interesting segments of optical information processing must be the image subtraction. The applications may be of value in earth resource studies, urban development, highway planning, land use, surveillance, automatic tracking, and many others. The image subtraction may also be applied to video communications as a means of bandwidth compression. For example it is only necessary to transmit the differences between the two images in successive cycles, rather than the entire image in each cycle.

There are several techniques available for image subtraction which can be found in a review paper by Ebersole [1]. However most of the optical image subtraction techniques have relied on a coherent source to carry out the subtraction operation. But a coherent optical processing system is plagued with coherent noise, which frequently limits its processing capabilities.

We have in a recent paper [2] demonstrated a technique of image subtraction utilizing an extended incoherent source. Since the image subtraction is a one-dimensional processing operation and the spatial coherence requirement for the subtraction operation is a point-pair coherence requirement, it is, therefore, possible to encode an extended source to obtain the required spatial coherence. In a previous paper [3] we have shown a Fourier transform relationship between the spatial coherence and source intensity distribution. In principle, it is possible to encode an extended source to obtain an appropriate spatial coherence for specific information processing operations.

Strictly speaking, all images in the visible wavelengths, which includes the black-and-white images, are color images. Therefore it is of interest for us, in this paper, to extend this incoherent processing technique for color image subtraction.

II. — COLOR IMAGE SUBTRACTION

We will now describe a color image subtraction operation with an encoded extended incoherent source, as depicted in *figure 1*. For simplicity, two

(*) Visiting scholar from *Shanghai Institute of Optics and Fine Mechanics*, Academia Sinica (China).

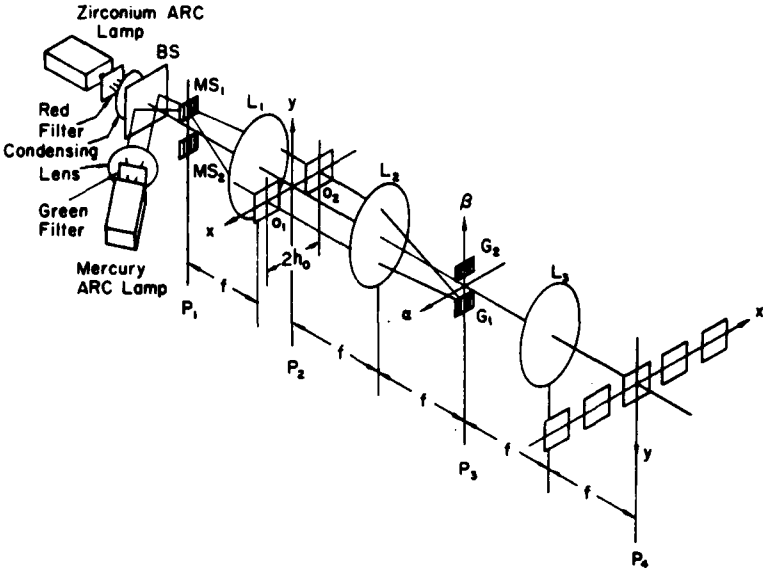

FIG. 1. — *Color Image Subtraction with Encoded Extended Incoherent Sources. BS ; Beam Spliter, MS ; Source Encoding Mask, L ; Achromatic Transform Lens, G ; Diffraction Gratings.*

incoherent light sources, each for a different color of light (*i.e.*, red and green), are used for the subtraction operation. For the detailed analysis of image subtraction with an encoded extended source we refer the reader to our previous paper [2].

In color image subtraction, we insert the color image transparencies $O_1(x, y)$ and $O_2(x, y)$ in the open apertures of the input plane P_2, which can be described as

$$(1) \quad f(x, y) = O_1(x - h_0, y) + O_2(x + h_0, y) ,$$

where $2 h_0$ is the separation between the two input transparencies O_1 and O_2. Two sinusoidal gratings G_1 and G_2 designed for the red and the green color wavelengths respectively are inserted in the spatial frequency plane P_3, and can be written as

$$(2) \qquad G_1 = \frac{1}{2}[1 + \sin(h_0 p_r)] ,$$

and

$$(3) \qquad G_2 = \frac{1}{2}[1 + \sin(h_0 p_g)] ,$$

where $p_r = (2\pi\alpha)/(\lambda_r f)$ and $p_g = (2\pi\alpha)/(\lambda_g f)$ are the spatial frequencies of the gratings, λ_r and λ_g are the red and green color wavelengths, α denotes the spatial coordinate in the same direction as p, and f is the focal length of the achromatic transform lens L_2. By a straight-forward but rather cumbersome evaluation, the irradiance around the origin of the output image plane P_4 can be shown [2],

$$(4) \quad I(x, y) = I_r(x, y) + I_g(x, y) = K\,|\,O_{1_r}(x, y) - O_{2_r}(x, y)\,|^2 + K\,|\,O_{1_g}(x, y) - O_{2_g}(x, y)\,|^2 ,$$

where $I_r(x, y)$ and $I_g(x, y)$ denote the red and green subtracted color image irradiances, O_{1_r}, O_{2_r}, O_{1_g} and O_{2_g} are the corresponding red and green color input objects. From Eq. (4) we see that the subtracted color image can be obtained at the output image plane. Since the color image subtraction is obtained with extended incoherent sources, the coherent artifact noise can be suppressed.

III. — SOURCE ENCODING FOR IMAGE SUBTRACTION

We would now consider a source encoding technique for image subtraction. As we have pointed out earlier, the image subtraction is a $1 - D$ processing operation and the spatial coherence requirement is dependent upon corresponding image points to be subtracted. Therefore, instead of utilizing a strictly broad spatial coherence function, a point-pair spatial coherence is sufficient. To insure a physically realizable source intensity distribution, we let the point-pair spatial coherence be [2, 3]

$$(5) \quad \Gamma(|\,x - x'\,|) = \frac{\sin\left(\frac{N\pi}{h_0}\,|\,x - x'\,|\right)}{N \sin\left(\frac{\pi}{h_0}\,|\,x - x'\,|\right)} \times \operatorname{sinc}\left(\frac{\pi w}{h_0 d}\,|\,x - x'\,|\right) ,$$

where $2 h_0$ is the separation between the image points, $N \gg 1$ a positive integer, and $w \ll d$. The first factor of Eq. (5) represents a sequence of narrow pulses present at every $|\,x - x'\,| = nh_0$, where n is a positive

integer, and the peak values of the pulses are weighted by a broader sinc factor, as shown in *figure 2(a)*. From this figure, we see that there exists a high degree of spatial coherence between every point-pair of the two input objects O_1 and O_2. By taking the Fourier transformation of Eq. (5), we obtain the following intensity distribution [3]

$$S(|x|) = \sum_{n=1}^{N} \text{rect}\left(\frac{|x - nd|}{w}\right), \tag{6}$$

where w is the slit width, $d = (\lambda f)/h_0$ is the separation between the slits of the source coding apertures, λ is the wavelength of the light source, and f is the focal length of the collimating lens. Thus the intensity distribution of Eq. (6) represents N number of narrow slit apertures with equal spacing d, as shown in *figure 2(b)*. From this result, it is possible to encode an extended source to obtain a spatial coherence function at the input plane for the subtraction operation.

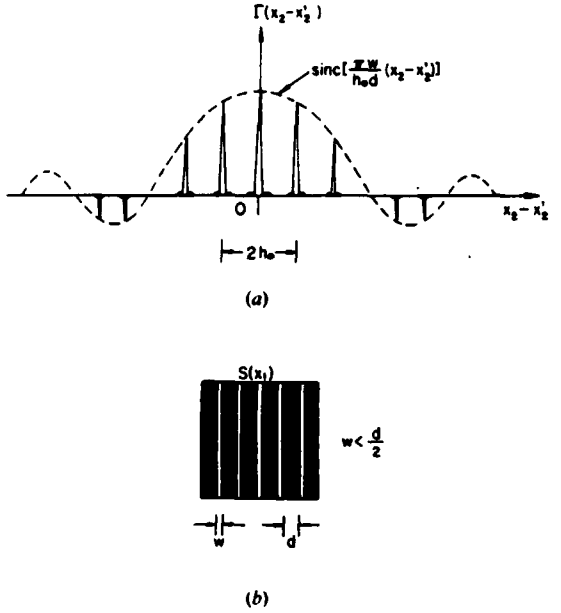

FIG. 2. — (a) *A Point-pair Spatial Coherence Function.* (b) *Source Encoding Mask.*

Since the scale of the Fourier spectrum varies with the wavelength of the light source, a temporal coherence requirement should also be imposed on every processing operation. In other words, the spectral width (*i.e.*, temporal coherence) of the light source should be restricted by the following inequality [3]

$$\frac{\Delta\lambda}{\lambda} \ll \frac{\pi}{h_0 p_m}, \tag{7}$$

where λ is the center wavelength of the light source and p_m is the highest angular spatial frequency required for the image subtraction. Consequently, if the spatial frequency requirement is high, then a narrow spectral width of the light source is required.

IV. — EXPERIMENTAL DEMONSTRATION

Strictly speaking, light sources emitting all primary colors (*i.e.*, red, green, and blue) should be used for the color images subtraction. For simplicity of experimental demonstration, a mercury arc lamp with a green filter (5 461 Å) and a zirconium arc lamp with a red filter (6 328 Å) were used for the color light sources. The intensity ratio of the two resulting light sources was adjusted to about unity with a variable beam splitter.

The slit widths for the source encoding masks were about 2.5 μ and the spacings of the slits were 25 μ for the green wavelength and 29 μ for the red wavelength. The overall size of the source encoding masks was about 3×3 mm^2 which contained about 120 and 100 slits respectively. The focal length of the transform lenses was 300 mm. A liquid gate containing two color image transparencies about 6×8 mm^2 each and with a separation of about 13.2 mm was placed behind the collimator. Two sinusoidal gratings with spatial frequencies of 1/(25 μ) and 1/(29 μ) were used for the green and red color image subtraction operation, as shown in *figure 1*.

In our first experimental demonstration, we provide in *figures 3(a)* and *3(b)* two sets of different colored

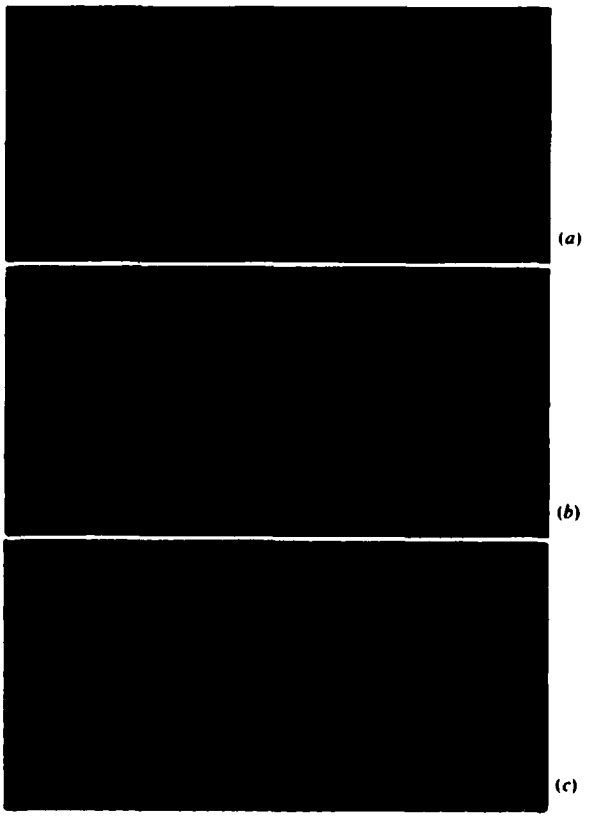

FIG. 3. — *Color Image Subtraction; Binary Object.* (a) *et* (b) *Input Color English Words.* (c) *Subtracted Color Image.*

English words as input objects. *Figure 3(c)* shows the subtracted color image obtained with the color subtraction technique. The input words *STATE UNIV.* are red and green respectively in one set but they are green and red respectively in the other set while in the subtracted image, as shown in *figure 3(c)*, both words are in yellow color, which is consistent with the result we expected. In other words, the subtracted image of red and green produces yellow color since the red and green wavelengths are incoherent and therefore add incoherently to produce a yellow color.

For a second demonstration, we provide two continuous tone color images of two sets of fruit, as shown in *figures 4(a)* and *4(b)*. By comparing these two figures, we see that a dark green cucumber and a red tomato are missing in *figure 4(b)*. *Figure 4(c)* shows the subtracted color image obtained with this incoherent color image subtraction technique. In this result, the profiles of a cucumber and a tomato can be seen at the output image plane.

For the final demonstration, we again provide two continuous tone color images of a parking lot as input color object transparencies, as shown in *figures 5(a)* and *5(b)*. From these input transparencies, we see that a red color passenger car shown in the parking lot in *figure 5(a)* is missing in *figure 5(b)*. *Figure 5(c)* is the color subtracted image obtained from the incoherent color image subtraction technique as previously described. In this figure, a red passenger car can clearly be seen at the output image plane. It is also interesting to point out that the parking line (in yellow color) on the right side of the red car can readily be seen with the subtracted image.

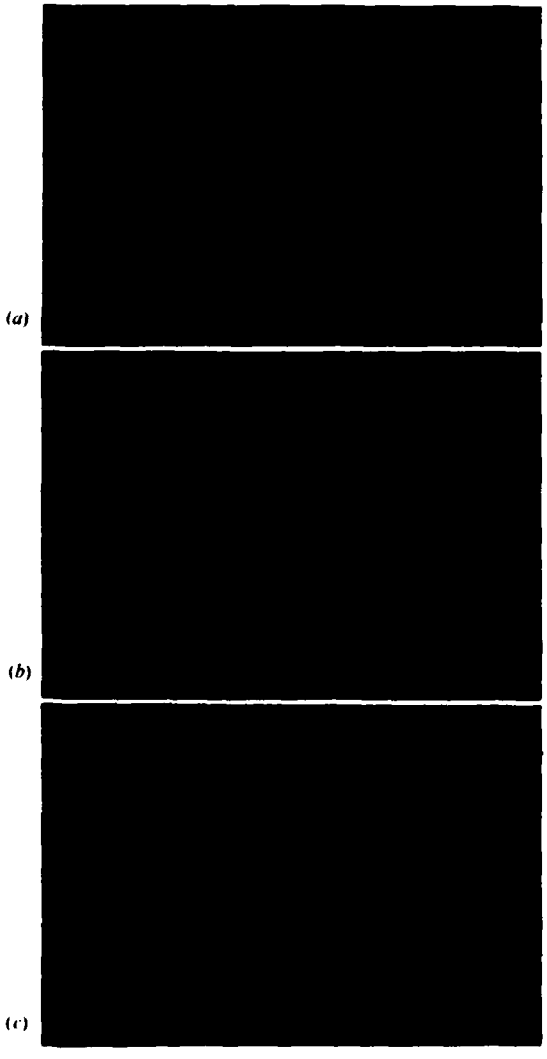

FIG. 4. — *Color Image Subtraction; Continuous Tone Object.* (a) *et* (b) *Input Color Object Transparencies Subtracted Color Image.*

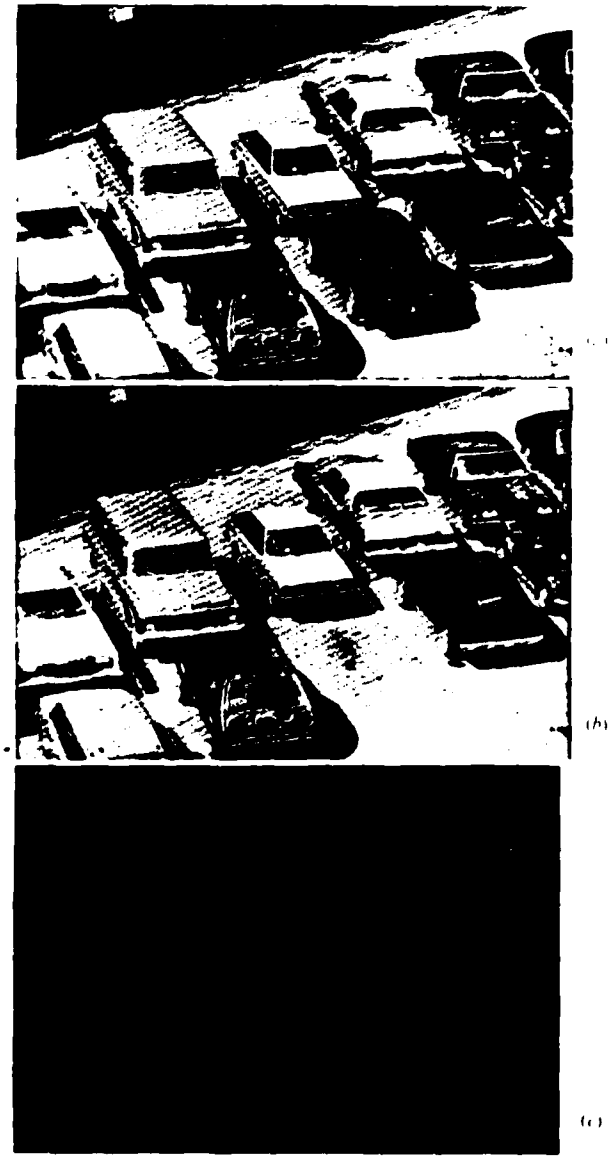

FIG. 5. *Color Image Subtraction, Parking Lot.* (a) *et* (b) *Input Color Transparencies.* (c) *Subtracted Color Image*

V. — *CONCLUSION*

We have introduced a color image subtraction technique with encoded incoherent sources. The basic advantage of source encoding is to increase the available light power for the image subtraction operation, so that the inherent difficulty of obtaining incoherent point sources can be alleviated. Since the technique uses incoherent sources, the annoying coherent artifact noise can be suppressed. We would see that the concept of color image subtraction may also be extended to the use of white-light source, for which a program is currently under investigation. In experimental demonstrations, we have shown that color subtracted images can be easily obtained by this incoherent subtraction technique. Since virtually all images of natural objects are color, the technique may offer a wide range of practical applications.

REFERENCES

[1] EBERSOLE (J. F.). — *Opt. Eng.*, 1975, *14*, 436
[2] WU (S. T.), YU (F. T. S.). — *Appl. Opt.* (*to be published*).
[3] YU (F. T. S.), ZHUANG (S. L.), WU (S. T.). — *Appl. Phys.* (*to be published*).

The authors wish to acknowledge the support by *U.S. Air Force Office* of Scientific Research Grant AFSOR-81-0148.

(Manuscript received in August 3, 1981)

SECTION VII

Rainbow Holographic Aberrations

Reprinted from Applied Optics, Vol. 22, page 164, January 1, 1983

Rainbow holographic aberrations and the bandwidth requirements

Y. W. Zhang, W. G. Zhu, and F. T. S. Yu

Rainbow holographic image resolution, primary aberrations, and bandwidth requirements are presented. The results obtained for the rainbow holographic process are rather general, for which the conventional holographic image resolution, aberrations, and bandwidth requirements, can be derived. The conditions for the elimination of the five primary rainbow holographic aberrations are also given. These conditions may be useful for the application of obtaining a high-quality rainbow hologram image. In terms of bandwidth requirements, we have shown that the bandwidth requirement for a rainbow holographic construction is usually several orders lower than that of a conventional holographic process. Therefore, a lower-resolution recording medium can generally be used for most of the rainbow holographic constructions.

I. Introduction

The rainbow holographic process of Benton[1] involves two recording steps. First, a primary hologram is made from a real object with the conventional off-axis holographic techniques, and second, the rainbow hologram is recorded from the real hologram image from the primary hologram. The relaxation of the coherence requirement on the reconstructing process arises from the placement of a narrow slit behind the primary hologram in the second-step holographic recording. However, the two-step holographic recording process is cumbersome and requires a separate optical setup for each step. It is usually a major undertaking for laboratories with limited optical components. An alternative method of obtaining a rainbow hologram is the one-step process of Chen *et al.*[2-5] They had shown that the one-step technique offers certain flexibilities, and the optical arrangement is simpler than the conventional two-step process. We also note that the color blur of the Benton type rainbow hologram has been subsequently analyzed by Wyant,[6] Chen,[7] and Tamura.[8] Recently, Zhuang *et al.*[9] investigated the image resolution and color blur for a one-step rainbow holographic process utilizing diffraction optics.

In this paper, we shall evaluate the primary aberrations and bandwidth requirement for a rainbow holographic process. The correlations for the elimination of the rainbow holographic aberrations are presented.

The authors are with Pennsylvania State University Electrical Engineering Department, University Park, Pennsylvania 16802.
Received 20 August 1982.
0003-6935/83/010164-06$01.00/0.

Since the effective aperture of a rainbow hologram is generally smaller than that of a conventional hologram, the spatial bandwidth requirement is generally somewhat lower for the rainbow holographic process. Therefore, it is usually possible to construct a rainbow hologram utilizing a lower-resolution film.

II. Rainbow Holographic Resolution

In a recent paper,[6] the resolution limit and color blur of a rainbow hologram were analyzed from diffraction optics. However, in practice, the slit used in a rainbow holographic process is many orders larger than the light wavelength. Therefore, the rainbow holographic process can also be approached from slightly different configurations as depicted in Fig. 1. For simplicity, both the recording and the reconstruction processes are drawn in a composite diagram, where H_1 represents the primary hologram which is in contact with a narrow-slit aperture SL, H_2 represents the constructing rainbow hologram, $O(x_0,y_0)$ is the object image point, $I(x_i,y_i)$ is the rainbow hologram image point, and $R(x_r,y_r)$ and $C(x_c,y_c)$ are the reference and the reconstruction point sources, respectively. We note that if O and SL represent the object and slit images due to an imaging lens, the same diagram of Fig. 1 can also be used for the analysis of a one-step rainbow holographic process.

With reference to Fig. 1, it is evident that the coordinate points P_{11} and P_{12} are the marginal extensions of the rainbow holographic recording region, which can be written as

$$P_{11} = \left(1 - \frac{d}{g}\right) x_0 + \frac{dw}{2g}, \tag{1}$$

$$P_{12} = \left(1 - \frac{d}{g}\right) x_0 - \frac{dw}{2g}, \tag{2}$$

where $g \triangleq s + d$.

Thus, the complex light-amplitude distribution due to the object image point O at the rainbow holographic recording plate H_2 is

$$U_1(x;k_1) = A_1 \exp\{-ik_1[d^2 + (x - x_0)^2]^{1/2}\}, \quad (3)$$

and the corresponding complex light distribution due to the reference and reconstructing (called illuminating) beams are

$$U_2(x;k_1) = A_2 \exp\{-ik_1[L_1^2 + (x - x_r)^2]^{1/2}\}, \quad (4)$$

$$U_3(x;k_2) = A_3 \exp\{-ik_2[L_2^2 + (x - x_c)^2]^{1/2}\}, \quad (5)$$

respectively, where the spatial impulse response is

$$h_l(\alpha - x;k_2) = A_4 \exp\{ik_2[l^2 + (\alpha - x)^2]^{1/2}\}, \quad (6)$$

Ai is a complex constant, $k = 2\pi/\lambda$, and λ_1 and λ_2 are the wavelengths for the rainbow hologram construction and the reconstructing processing, respectively.

The corresponding complex light field of the rainbow hologram image point I is

$$B_i(\alpha;k_2) = C_1 \int_{P_{12}}^{P_{11}} U_1 U_2^* U_3 h_l dx = C_2 \operatorname{sinc}\left[\frac{dw}{\lambda_2 g l_i}(\alpha + \alpha_i)\right], \quad (7)$$

where

$$l_i = \frac{dL_1L_2}{\mu L_1L_2 + dL_1 - \mu dL_2}, \quad (8)$$

$$\alpha_i = l_i\left(-\mu\frac{x_0}{d} - \frac{x_c}{L_2} + \mu\frac{x_r}{L_1}\right), \quad (9)$$

(l_i,α_i) identifies the position of the rainbow hologram image point I, and $\mu \triangleq \lambda_2/\lambda_1$.

The magnification of the hologram image can then be written as

$$M_i = \frac{\alpha_i}{x_0} = \frac{\mu l_i}{d} = \left(1 - \frac{d}{L_1} + \frac{d}{\mu L_2}\right)^{-1}, \quad (10)$$

and the resolution limit of the rainbow holographic process is

$$\Delta H_i = \frac{\lambda_2 l_i\left(1 + \frac{s}{d}\right)}{W} = \frac{\lambda_2 L_1 L_2(d + s)}{(\mu L_1 L_2 + L_1 d - \mu L_2 d)W}, \quad (11)$$

where W is the slit width. If both the reference and the reconstruction beams are plane waves, the resolution limit becomes

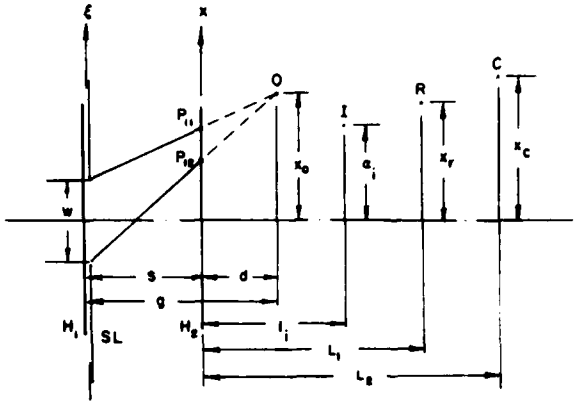

Fig. 1. A composite rainbow holographic construction and reconstruction process for the evaluation of the hologram image resolution and the primary aberrations: H_1, primary hologram; SL, slit aperture; W, slit width; H_2, rainbow holographic plate; O, object image point; I, rainbow hologram image point; R, convergent reference point source; C, white-light reconstruction point source.

$$\Delta H_i = \frac{\lambda_1(d + s)}{W}. \quad (12)$$

We note that these results are identical to the results we obtained previously by Zhuang *et al.*[10] It is evident that this partial geometrics approach simplifies the rainbow holographic analysis.

III. Rainbow Holographic Aberrations

In evaluating the rainbow holographic aberration, we expand the exponent of Eq. (7) in binomial expansion such as

$$\varphi(x,k) = k[L^2 + (x - a)^2]^{1/2} = k\left[1 + \frac{(x - a)^2}{2L} - \frac{(x - a)^4}{8L^3} + \ldots\right]. \quad (13)$$

Thus, by retaining the first three terms of Eq. (13), the third-order primary aberrations of a rainbow holographic process can be obtained.

To evaluate the third-order primary aberrations, the phase factor of the real rainbow hologram image can be written as

$$\varphi_i = k_2\mu[L_1^2 + (x - x_r)^2 + (y - y_r)^2]^{1/2} - \mu[d^2 + (x - x_0)^2 + (y - y_0)^2]^{1/2} - [L_2^2 + (x - x_c)^2 + (y - y_c)^2]^{1/2} + [l_i^2 + (\alpha_i - x)^2 + (\beta_i - y)^2]^{1/2}]. \quad (14)$$

With reference to the binomial expansion of Eq. (13), Eq. (14) can be written as a configuration of the order terms, i.e.,

$$\varphi_i = \varphi_c + \varphi_p + \varphi_t + \varphi_h, \quad (15)$$

where ϕ_c, ϕ_p, and ϕ_h are the first-, second-, and higher-order terms, which shall be ignored in our evaluation. The third-order term, ϕ_t, is written as

$$\varphi_t = \frac{k_2}{8}\left\{\frac{\mu}{d^3}[(x - x_0)^2 + (y - y_0)^2]^2 - \frac{\mu}{L_1^3}[(x - x_r)^2 + (y - y_r)^2]^2 + \frac{1}{L_2^3}[(x - x_c)^2 + (y - y_c)^2]^2 - \frac{1}{l_i^3}[(\alpha_i - x)^2 + (\beta_i - y)^2]^2\right\}. \quad (16)$$

Table I. Rainbow Holographic Aberrations and the Conditions for Elimination

Name	Formula	Condition of eliminating aberration
Spherical	$S = \frac{\mu}{L_1^3} - \frac{\mu}{d^3} + \frac{1}{l_i^3} - \frac{1}{L_2^3}$	$\mu = 1; d = l_i; L_1 = L_2$
Coma	$C_x = \frac{\mu}{L_1^3} x_r - \frac{\mu}{d^3} x_0 + \frac{\alpha_i}{l_i^3} - \frac{x_c}{L_2^3}$	$\mu = 1; d = l_i; L_1 = L_2 = \infty$,
	$C_y = \frac{\mu}{L_1^3} y_r - \frac{\mu}{d^3} y_0 + \frac{\beta_i}{l_i^3} - \frac{y_c}{L_2^3}$	but, $\frac{x_r}{L_1}, \frac{y_r}{L_1}, \frac{x_c}{L_2}, \frac{y_c}{L_2}$ are finite
Astigmatism	$A_x = \frac{\mu x_r^2}{L_1^3} - \frac{\mu x_0^2}{d^3} + \frac{\alpha_i^2}{l_i^3} - \frac{x_c^2}{L_2^3}$ $A_{xy} = \frac{\mu x_r y_r}{L_1^3} - \frac{\mu x_0 y_0}{d^3} + \frac{\alpha_i \beta_i}{l_i^3} - \frac{x_c y_c}{L_2^3}$ $A_y = \frac{\mu y_r^2}{L_1^3} - \frac{\mu y_0^2}{d^3} + \frac{\beta_i^2}{l_i^3} - \frac{y_c^2}{L_2^3}$	$\mu = 1; d = l_i; L_1 = L_2 = \infty$, but, $\frac{x_r}{L_1}, \frac{y_r}{L_1}, \frac{x_c}{L_2}, \frac{y_c}{L_2}$ are finite
Curvature of field	$F = \frac{\mu}{L_1^3}(x_r^2 + y_r^2) - \frac{\mu}{d^3}(x_0^2 + y_0^2)$ $+ \frac{1}{l_i^3}(\alpha_i^2 + \beta_i^2) - \frac{1}{L_2^3}(x_c^2 + y_c^2)$	$\mu = 1; d = l_i; L_1 = L_2 = \infty$, but, $\frac{x_r}{L_1}, \frac{y_r}{L_1}, \frac{x_c}{L_2}, \frac{y_c}{L_2}$ are finite
Distortion	$D_x = \frac{\mu}{L_1^3} x_r^3 - \frac{\mu}{d^3} x_0^3 + \frac{\alpha_i^3}{l_i^3} - \frac{x_c^3}{L_2^3}$ $D_y = \frac{\mu}{L_1^3} y_r^3 - \frac{\mu}{d^3} y_0^3 + \frac{\beta_i^3}{l_i^3} - \frac{y_c^3}{L_2^3}$	$\mu = 1; \frac{x_r}{L_1} = \frac{x_c}{L_2}; \frac{y_r}{L_1} = \frac{y_c}{L_2}$

By substituting the relation of $x = r\cos\theta$ and $y = r\sin\theta$ into Eq. (16), the third-order phase factor can be shown as

$$\begin{aligned}\varphi_t = k_2 \Bigg\{ & \frac{1}{8}\left(\frac{\mu}{d^3} - \frac{\mu}{L_1^3} + \frac{1}{L_2^3} - \frac{1}{l_i^3}\right) r^4 - \frac{1}{2}\left[\left(\frac{\mu}{d^3} x_0 - \frac{\mu}{L_1^3} x_r \right.\right. \\ & \left. + \frac{x_c}{L_2^3} - \frac{\alpha_i}{l_i^3}\right)\cos\theta + \left(\frac{\mu}{d^3} y_0 - \frac{\mu}{L_1^3} y_r + \frac{y_c}{L_2^3} - \frac{\beta_i}{l_i^3}\right)\sin\theta \Bigg] r^3 \\ & + \frac{1}{4}\left[\frac{\mu}{d^3}(x_0^2 + y_0^2) - \frac{\mu}{L_1^3}(x_r^2 + y_r^2) + \frac{1}{L_2^3}(x_c^2 + y_c^2)\right. \\ & \left. - \frac{1}{l_i^3}(\alpha_i^2 + \beta_i^2)\right] r^2 + \frac{1}{2}\left[\left(\frac{\mu}{d^3} x_0^2 - \frac{\mu}{L_1^3} x_r^2 + \frac{x_c^2}{L_2^3} - \frac{\alpha_i^2}{l_i^3}\right)\cos^2\theta \right. \\ & + \left(\frac{\mu}{d^3} y_0^2 - \frac{\mu}{L_1^3} y_r^2 + \frac{y_c^2}{L_2^3} - \frac{\beta_i^2}{l_i^3}\right)\sin^2\theta + \left(\frac{\mu}{d^3} x_0 y_0 \right. \\ & \left.\left. - \frac{\mu}{L_1^3} x_r y_r + \frac{1}{L_2^3} x_c y_c - \frac{1}{l_i^3}\alpha_i\beta_i\right)\sin\theta\cos\theta\right] r^2 \\ & - \frac{1}{2}\left[\left(\frac{\mu}{d^3} x_0^3 - \frac{\mu}{L_1^3} x_r^3 + \frac{1}{L_2^3} x_c^3 - \frac{1}{l_i^3}\alpha_i^3\right)\cos\theta + \left(\frac{\mu}{d^3} y_0^3 \right.\right. \\ & \left.\left. - \frac{\mu}{L_1^3} y_r^3 + \frac{1}{L_2^3} y_c^3 - \frac{1}{l_i^3}\beta_i^3\right)\sin\theta\right] r\Bigg\}. \end{aligned} \tag{17}$$

Thus, φ_t can be written as a function of the five primary aberrations[10] such as

$$\begin{aligned}\varphi_t = k_2 \Bigg[& -\frac{r^4}{8} S + \frac{r^3}{2}(C_x\cos\theta + C_y\sin\theta) - \frac{r^2}{4} F \\ & - \frac{r^2}{2}(A_x\cos^2\theta + 2A_{xy}\sin\theta\cos\theta + A_y\sin^2\theta) \\ & + \frac{r}{2}(D_x\cos\theta + D_y\sin\theta)\Bigg], \end{aligned} \tag{18}$$

where S represents the spherical aberrations, C_x and C_y represent the meridian and tangential coma, A_x, A_{xy}, and A_y are the astigmatisms, F is the curvature of field, and D_x and D_y are the horizontal and vertical distortions. By comparing this equation with Eq. (17), the equations for the five primary rainbow holographic aberrations can be obtained as tabulated in Table I.

In this table, the conditions for the elimination of the primary aberrations are given. It is evident that all the primary aberrations can be eliminated if both the reference and the reconstruction beams are plane waves and $\mu = 1$. It is interesting to note that, if the slit width W is equal to the size of the primary hologram, by letting $S = 0$, the primary aberrations reduce to the conventional off-axis holographic aberrations as obtained by Meier.[11]

Since the rainbow holographic imaging is generally produced by a white-light source, the aberrations are

affected by the wavelength spread $\Delta\lambda_2$ during the reconstruction process. We note that this wavelength spread $\Delta\lambda_2$ is limited by observer eye through the slit image. Thus, the effect of aberration variation due to $\Delta\lambda_2$ can be determined as shown in the following, for simplicity as a 1-D notation:

$$\Delta S = \left(1 - \frac{\Delta\lambda_2}{\lambda_2}\right)\left[S - \frac{\Delta\lambda_2}{\lambda_1}\left(\frac{1}{L_1^2} - \frac{1}{d^2}\right) + \frac{\partial}{\partial\lambda_2}\left(\frac{1}{l_1^2}\right)\Delta\lambda_2\right] - S$$
$$\simeq -\frac{\Delta\lambda_2}{\lambda_2}S + \frac{\Delta\lambda_2}{\lambda_1}\left[\left(\frac{1}{L_1^2} - \frac{1}{d^2}\right) + \frac{L_2(L_1 - d)(\mu L_1 L_2 + L_1 d - \mu L_2 d)^2}{(dL_1L_2)^3}\right]. \tag{19}$$

$$\Delta C_x = \left(1 - \frac{\Delta\lambda_2}{\lambda_2}\right)\left\{C_x - \left(\frac{x_0}{d^3} - \frac{x_r}{L_1^3}\right)\frac{\Delta\lambda_2}{\lambda_1} - \frac{\Delta\lambda_2}{\lambda_1}\left[\frac{1}{l_1^2}\left(\frac{x_0}{d} - \frac{x_r}{L_1}\right)\right.\right.$$
$$\left.\left. + \frac{2L_2(L_1 - d)}{l_1^2(\mu L_1 L_2 + L_1 d - \mu L_2 d)}\left(\mu\frac{x_0}{d} + \frac{x_c}{L_2} - \mu\frac{x_r}{L_1}\right)\right]\right\} - C_x$$
$$\simeq -\frac{\Delta\lambda_2}{\lambda_2}C_x + \frac{\Delta\lambda_2}{\lambda_1}\left\{\left(\frac{x_r}{L_1^3} - \frac{x_0}{d^3}\right) - \frac{1}{l_1^2}\left[\left(\frac{x_0}{d} - \frac{x_r}{L_1}\right)\right.\right.$$
$$\left.\left. + \frac{2L_2(L_1 - d)}{(\mu L_1 L_2 + L_1 d - \mu L_2 d)}\left(\mu\frac{x_0}{d} + \frac{x_c}{L_2} - \mu\frac{x_r}{L_1}\right)\right]\right\}. \tag{20}$$

$$\Delta F = \Delta A_x = \left(1 - \frac{\Delta\lambda_2}{\lambda_2}\right)\left\{F + \left(\frac{x_r^2}{L_1^3} - \frac{x_0^2}{d^3}\right)\frac{\Delta\lambda_2}{\lambda_1} + \frac{\Delta\lambda_2}{\lambda_1 dL_1L_2}\left[L_2(L_1 - d)\left(\mu\frac{x_0}{d} + \frac{x_c}{L_2} - \mu\frac{x_r}{L_1}\right)^2 + 2(\mu L_1L_2 + L_1d - \mu L_2d)\left(\mu\frac{x_0}{d}\right.\right.\right.$$
$$\left.\left.\left. + \frac{x_c}{L_2} - \mu\frac{x_r}{L_1}\right)\left(\frac{x_0}{d} - \frac{x_r}{L_1}\right)\right]\right\} - F \simeq -\frac{\Delta\lambda_2}{\lambda_2}F + \frac{\Delta\lambda_2}{\lambda_1}\left\{\left(\frac{x_r^2}{L_1^3}\right.\right.$$
$$\left.\left. - \frac{x_0^2}{d^3}\right) + \frac{\left(\mu\frac{x_0}{d} + \frac{x_c}{L_2} - \mu\frac{x_r}{L_1}\right)}{dL_1L_2}\left[L_2(L_1 - d)\left(\mu\frac{x_0}{d} + \frac{x_c}{L_2}\right.\right.\right.$$
$$\left.\left.\left. - \mu\frac{x_r}{L_1}\right) + 2\left(\frac{x_0}{d} - \frac{x_r}{L_1}\right)(\mu L_1L_2 + L_1d - \mu L_2d)\right]\right\}. \tag{21}$$

$$\Delta D_x = \left(1 - \frac{\Delta\lambda_2}{\lambda_2}\right)\left\{D_x + \left[\left(\frac{x_r^3}{L_1^3} - \frac{x_0^3}{d^3}\right) - 3\left(\mu\frac{x_0}{d} + \frac{x_c}{L_2} - \mu\frac{x_r}{L_1}\right)^2\left(\frac{x_0}{d}\right.\right.\right.$$
$$\left.\left.\left. - \frac{x_r}{L_1}\right)\right]\frac{\Delta\lambda_2}{\lambda_1}\right\} - D_x \simeq -\frac{\Delta\lambda_2}{\lambda_2}D_x + \frac{\Delta\lambda_2}{\lambda_1}\left(\frac{x_r}{L_1}\right.$$
$$\left. - \frac{x_0}{d}\left[\left(\frac{x_0^2}{d^2} + \frac{x_0x_r}{dL_1} + \frac{x_r^2}{L_1^2}\right) + 3\left(\mu\frac{x_0}{d} + \frac{x_c}{L_2} - \mu\frac{x_r}{L_1}\right)^2\right]\right). \tag{22}$$

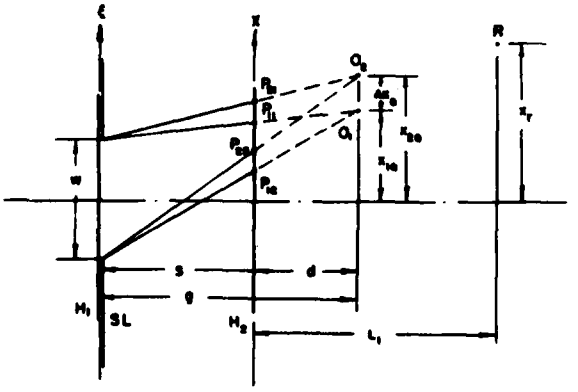

Fig. 2. A composite rainbow holographic construction and reconstruction process for determining the bandwidth requirements: H_1, primary hologram; SL, slit aperture; W, slit width; H_2, rainbow holographic plate; O_1–O_2, extended hologram object image; R, convergent reference point source.

From Eq. (21) we see that the variation of the astigmatism is identical to that of the variation of curvature of field. In ending this section, we point out that the above equations have useful applications for evaluating the rainbow hologram image quality.

IV. Bandwidth Requirements

Since the effective aperture of a rainbow hologram is generally smaller than that of a conventional hologram, it is possible that a lower-resolution film can be utilized. Therefore, it is our aim in this section to discuss the bandwidth requirements of a rainbow holographic process.

We shall investigate for the case in which the slit and the object image are located at opposite sides of the rainbow holographic plots H_2 as shown in Fig. 2, where O_1 and O_2 are the two external points of an extended object image reconstructed from a primary hologram H_1. Thus, from Fig. 2, we see that

$$P_{11} = \left(1 - \frac{d}{g}\right)x_{01} + \frac{d}{2g}W,$$
$$P_{12} = \left(1 - \frac{d}{g}\right)x_{01} - \frac{d}{2g}W,$$
$$P_{21} = \left(1 - \frac{d}{g}\right)x_{02} + \frac{d}{2g}W, \tag{23}$$
$$P_{22} = \left(1 - \frac{d}{g}\right)x_{02} - \frac{d}{2g}W.$$

Similar to what we did in previous sections, the complex light fields U_1, U_2, and U_3 due to the object image points O_1 and O_2 and the reference beam R can be formulated. The terms contributing to the rainbow holographic reconstruction process are

$$U_1U_3^* + U_3U_1^* = 2|A_1||A_3| \cos\left\{k_1\left[L_1 - d - \frac{(x - x_{01})^2}{2d} + \frac{(x - x_r)^2}{2L_1}\right] + \theta_1\right\}, \quad (24)$$

$$U_2U_3^* + U_3U_2^* = 2|A_2||A_3| \cos\left\{k_1\left[L_1 - d - \frac{(x - x_{02})^2}{2d} + \frac{(x - x_r)^2}{2L_1}\right] + \theta_2\right\}, \quad (25)$$

where A_1, A_2, and A_3 are the complex constants, and θ_1 and θ_2 are the constant phase factors. The phase shifts due to the U_1, U_2, and U_3 are

$$\varphi_{31} = k_1\left[L_1 - d - \frac{(x - x_{01})^2}{2d} + \frac{(x - x_r)^2}{2L_1}\right] + \theta_1, \quad (26)$$

$$\varphi_{32} = k_1\left[L_1 - d - \frac{(x - x_{02})^2}{2d} + \frac{(x - x_r)^2}{2L_1}\right] + \theta_2, \quad (27)$$

respectively.

The derivatives of ϕ_{31} and ϕ_{32} represent the angular spatial frequency along the x direction. Thus, the corresponding linear spatial frequencies are

$$\nu_{31} = \frac{1}{2\pi}\frac{d\varphi_{31}}{dx} = \frac{1}{\lambda_1}\left[\left(\frac{1}{L_1} - \frac{1}{d}\right)x + \frac{x_{01}}{d} - \frac{x_r}{L_1}\right], \quad (28)$$

$$\nu_{32} = \frac{1}{2\pi}\frac{d\varphi_{32}}{dx} = \frac{1}{\lambda_1}\left[\left(\frac{1}{L_1} - \frac{1}{d}\right)x + \frac{x_{02}}{d} - \frac{x_r}{L_1}\right], \quad (29)$$

where ν denotes the spatial frequency. Therefore, the spatial frequency bandwidth of the rainbow hologram can be shown as

$$\Delta\nu = \nu_{32}|_{x=P_{12}} - \nu_{31}|_{x=P_{11}} = \frac{1}{\lambda_1 L_{1g}}[(L_1 + s)\Delta x_0 + (L_1 - d)W], \quad (30)$$

where $g = s + d$ and $\Delta x_0 = x_{02} - x_{01}$. If we let

$$\Delta\nu_1 = \frac{1}{\lambda_{1g}}\left(1 + \frac{s}{L_1}\right)\Delta x_0, \quad (31)$$

$$\Delta\nu_2 = \frac{1}{\lambda_{1g}}\left(1 - \frac{d}{L_1}\right)W, \quad (32)$$

Eq. (30) reduces to

$$\Delta\nu = \Delta\nu_1 + \Delta\nu_2, \quad (33)$$

where $\Delta\nu_1$ and $\Delta\nu_2$ are the spatial frequency bandwidths due to the size of object image and the slit of the rainbow holographic construction, respectively. Moreover, Eq. (30) can also be written as

$$\Delta\nu = \frac{1}{\lambda_{1g}}\left[\Delta x_0 + W + (s\Delta x_0 - dW)\frac{1}{L_1}\right]. \quad (34)$$

From this equation, we see that if $(\Delta x_0)/W > d/s$, increasing L_1 can compress the spatial frequency bandwidth of the rainbow hologram. On the other hand, if $(\Delta x_0)/W < d/s$, decreasing L_1 can also compress the spatial frequency bandwidth of the rainbow hologram. However, for the case $(\Delta x_0)/W = d/s$, the L_1 is independent of $\Delta\nu$.

Table II shows the spatial frequency bandwidth requirements for various rainbow holographic recording

Table II. Rainbow Holographic Bandwidth Requirements

L_1	Reference waveform	$\Delta\nu$
$L_1 = \infty$	plane wave	$\frac{1}{\lambda_{1g}}(\Delta x_0 + W)$
$d < L_1 < \infty$	convergent	$\frac{1}{\lambda_{1g}}\left[\left(1 + \frac{s}{L_1}\right)\Delta x_0 + \left(1 - \frac{d}{L_1}\right)W\right]$
$L_1 = d$	convergent	$\frac{1}{\lambda_{1d}}\Delta x_0$
$P < L_1 < d$	convergent	$\frac{1}{\lambda_{1g}}\left[\left(1 + \frac{s}{L_1}\right)\Delta x_0 - \left(1 - \frac{d}{L_1}\right)W\right]$
$-s < L_1 < -P$	divergent	$\frac{1}{\lambda_{1g}}\left[\left(\frac{s}{\lvert L_1\rvert} - 1\right)\Delta x_0 + \left(1 + \frac{d}{\lvert L_1\rvert}\right)W\right]$
$L_1 = -s$	divergent	$\frac{1}{\lambda_{1s}}W$
$-\infty < L_1 < -s$	divergent	$\frac{1}{\lambda_{1g}}\left[\left(1 - \frac{s}{\lvert L_1\rvert}\right)\Delta x_0 + \left(1 + \frac{d}{\lvert L_1\rvert}\right)W\right]$
$L_1 = -\infty$	plane wave	$\frac{1}{\lambda_{1g}}(\Delta x_0 + W)$

conditions. In this table, the notation p denotes the distance from rainbow holographic plate H_2 with respect to the reference beam R, where the paraxial approximation holds.

We note that, for a 2-D case, the general formulas for spatial frequency bandwidth requirements for a rainbow holographic process can be written as

$$\Delta\nu_x = \frac{1}{\lambda_{1g}}\left[\left|1+\frac{s}{L_1}\right|\Delta x_0 + \left|1-\frac{d}{L_1}\right| W\right],$$
$$\Delta\nu_y = \frac{1}{\lambda_{1g}}\left[\left|1+\frac{s}{L_1}\right|\Delta y_0 + \left|1-\frac{d}{L_1}\right| L\right], \tag{35}$$

where $\Delta\nu_x$ and $\Delta\nu_y$ are the corresponding spatial frequency bandwidths in the x and y directions, respectively, for $\Delta X_0 > O$, $\Delta y_0 > O$, and $s > O$. It is interesting to note that if $s = O$, $W = L_x$, and $L = L_y$, which correspond to the recording conditions of a conventional hologram, Eq. (35) reduces to the results obtained by Yu,[12] i.e.,

$$\Delta\nu_x' = \frac{1}{\lambda_1 d}\left[\Delta x_0 + \left|1-\frac{d}{L_1}\right| L_x\right],$$
$$\Delta\nu_y' = \frac{1}{\lambda_1 d}\left[\Delta y_0 + \left|1-\frac{d}{L_1}\right| L_y\right]. \tag{36}$$

To have some feeling of magnitude, we would provide two numerical examples as given in the following:

(1) For conventional holograph construction process; we let $L_x = L_y = 100$ mm, $\Delta x_0 = \Delta y_0 = 60$ mm, d = 200 mm, $L_1 \to \infty$, and $\lambda_1 = 5 \times 10^{-4}$ mm. By substituting these data into Eq. (36), we obtain the following bandwidth requirements: $\Delta\nu_x' = \Delta\nu_y' = 1600$ lines/mm.

(2) For rainbow holographic construction process, we let $W = 7$ mm, $L = 100$ mm, $s = 830$ mm, $d = 40$ mm, $L_1 = 1000$ mm, $\lambda_1 = 5 \times 10^{-4}$ mm, and $\Delta x_0 = \Delta y_0 = 6$ mm. By substituting these data into Eq. (35), we obtain the following rainbow holographic bandwidth requirements for the x and y directions: $\Delta\nu_x = 40$ lines/mm, and $\Delta\nu_y = 246$ lines/mm. In comparison with these two numerical examples, we see that the bandwidth requirements for the rainbow holographic construction are somewhat lower than those of the conventional holographic process. Thus, in practice, a lower-resolution film can be utilized for rainbow hologram recording.

V. Conclusion

The image resolution and third-order primary aberrations of a rainbow holographic process were derived. The results that we have obtained are rather general, for which the resolution limits and the aberrations of a conventional holographic process can be derived from these results. The conditions for the elimination of the rainbow holographic aberrations were also presented. These conditions are very useful for controlling the rainbow holographic image quality.

The bandwidth requirement of a rainbow holographic process was also evaluated. As compared with the conventional holographic process, the bandwidth requirement for a rainbow holographic process is usually several orders lower than that of a conventional holographic process. Thus, in practice, a lower-resolution film can be utilized for most rainbow holographic constructions.

We wish to acknowledge S. L. Zhuang for his valuable comments and suggestions and the support of the U.S. Air Force Office of Scientific Research grant AFOSR-81-0148.

References

1. S. A. Benton, J. Opt. Soc. Am. **59**, 1545A (1969).
2. H. Chen and F. T. S. Yu, Opt. Lett. **2**, 85 (1978).
3. F. T. S. Yu and H. Chen, Opt. Commun. **25**, 173 (1978).
4. A. M. Tai, F. T. S. Yu, and H. Chen, Appl. Opt. **18**, 61 (1979).
5. F. T. S. Yu, A. M. Tai, and H. Chen. Opt. Eng. **19**, 666 (1980).
6. J. C. Wyant, Opt. Lett. **1**, 130 (1977).
7. H. Chen, Appl. Opt. **17**, 3290 (1978).
8. P. N. Tamura, Appl. Opt. **17**, 3343 (1978).
9. S. L. Zhuang, P. H. Ruterbusch, Y. W. Zhang, and F. T. S. Yu, Appl. Opt. **20**, 872 (1981).
10. M. Born and E. Wolf, Eds., *Principles of Optics* (Pergamon, New York, 1964).
11. R. W. Meier, J. Opt. Soc. Am. **55**, 989 (1965).
12. F. T. S. Yu, *Introduction to Diffraction Information Processing and Holography* (MIT Press, Cambridge, 1973).

VIII. LIST OF PUBLICATIONS RESULTING FROM AFOSR SUPPORT

1. S. T. Wu and F. T. S. Yu, "Source Encoding for Image Subtraction," Optics Letters, Vol. 6, pp. 452-454, September, 1981.

2. F. T. S. Yu and J. L. Horner, "Optical Processing of Photographic Images," Optical Engineering, Vol. 20, pp. 666-676, September-October 1981.

3. F. T. S. Yu, "Partially Coherent Optical Processing of Images," SPIE Proceedings on "Processing Images and Data from Optical Sensors," Vol. 292, pp. 2-8, 1982.

4. F. T. S. Yu and J. L. Horner, "Review of Optical Processing of Images," SPIE Proceedings on Processing Images and Data from Optical Sensors," Vol. 292, pp. 9-24, 1982.

5. F. T. S. Yu, S. L. Zhuang and T. H. Chao, "Color Photographic-Image Deblurring by White-Light Processing Technique," Journal of Optics, Vol. 13, pp. 57-61, March-April, 1982.

6. S. T. Wu and F. T. S. Yu, "Image Subtraction with Encoded Extended Incoherent Source," Applied Optics, Vol. 20, pp. 4082-4088, December 1981.

7. F. T. S. Yu, S. L. Zhuang and S. T. Wu, "Source Encoding for Partial Coherent Optical Processing," Applied Physics, Vol. B27, pp. 99-104, February 1982.

8. S. T. Wu and F. T. S. Yu, "Visualization of Color Coded Phase Object Variation with Incoherent Optical Processing Technique," Journal of Optics, Vol. 13, pp. 111-114, May-June, 1982.

9. S. L. Zhuang and F. T. S. Yu, "Coherence Requirement for Partially Coherent Optical Information Processing," Applied Optics, Vol. 21, pp. 2587-2595, July 1982.

10. F. T. S. Yu and S. T. Wu, "Color Image Subtraction with Encoded Extended Incoherent Source," Journal of Optics, 13, 183 (1982).

11. S. L. Zhuang and F. T. S. Yu, "Apparent Transfer Function for Partially Coherent Optical Information Processing," Applied Physics, B28, 359-366, August, 1982.

12. Y. W. Zhang, W. G. Zhu, and F. T. S. Yu, "Rainbow Holographic Aberrations and Bandwidth Requirements," Applied Optics, 22, 164 (1983).

13. F. T. S. Yu, X. X. Chen, and S. L. Zhuang, "Progress Report on Archival Storage of Color Films with White-Light Processing Technique," submitted to Applied Optics.

14. T. H. Chao, S. L. Zhuang, S. Z. Mao and F. T. S. Yu, "Broad Spectral Band Color Image Deblurring," Applied Optics (in press).

15. F. T. S. Yu, Optical Information Processing, Wiley-Interscience, N.Y., 1983.


DATE
ILME